WCAP 10538

TECHNICAL BASIS FOR ELIMINATING CLASS 1 ACCUMULATOR LINE RUPTURE AS THE STRUCTURAL DESIGN BASIS FOR CATAWBA UNITS 1 AND 2

S. A. Swamy
J. C. Schmertz
C. Y. Yang
A. D. Sane
R. A. Holmes

April 1984

APPROVED: _____
J. N. Chirigos, Manager
Structural Materials
Engineering

APPROVED: _____
E. R. Johnson, Manager
Structural and Seismic
Development

Work performed under Shop Order DXNJ 950

WESTINGHOUSE ELECTRIC CORPORATION
NUCLEAR ENERGY SYSTEMS
P.O. Box 355
Pittsburgh, Pennsylvania 15230

FOREWORD

This document contains Westinghouse Electric Corporation proprietary information and data which has been identified by brackets. Coding associated with the brackets set forth the basis on which the information is considered proprietary. These codes are listed with their meanings in WCAP-7211.

The proprietary information and data contained in this report were obtained at considerable Westinghouse expense and its release could seriously affect our competitive position. This information is to be withheld from public disclosure in accordance with the Rules of Practice, 10 CFR 2.790 and the information presented herein be safeguarded in accordance with 10 CFR 2.903. Withholding of this information does not adversely affect the public interest.

This information has been provided for your internal use only and should not be released to persons or organizations outside the Directorate of Regulation and the ACRS without the express written approval of Westinghouse Electric Corporation. Should it become necessary to release this information to such persons as part of the review procedure, please contact Westinghouse Electric Corporation, which will make the necessary arrangements required to protect the Corporation's proprietary interests.

The proprietary information is deleted in the unclassified version of this report.

TABLE OF CONTENTS

TABLE OF CONTENTS (cont'd)

TABLE OF CONTENTS (cont'd)

LIST OF FIGURES

LIST OF FIGURES (Cont'd.)

LIST OF TABLES

1.0 INTRODUCTION

1.1 BACKGROUND

The current structural design basis for the accumulator line requires postulating non-mechanistic circumferential (guillotine) breaks in which the pipe is assumed to rupture along the full circumference of the pipe. This results in overly conservative estimates of support loads. It is, therefore, highly desirable to be realistic in the postulation of pipe breaks for the accumulator line. Presented in this report are the descriptions of a mechanistic pipe break evaluation method and the analytical results that can be used for establishing that a guillotine type break wil' not occur within the Class 1 portions of the accumulator line. The evaluations considering circumferentially oriented flaws cover longitudinal cases.

1.2 SCOPE AND OBJECTIVE

The general purpose of this investigation is to show that a circumferential flaw which is larger than any flaw that would be present in the accumulator line will remain stable when subjected to the worst combination of plant loadings. The flaw stability criteria proposed for the analysis will examine both the global and local stability. The global analysis is carried out using the [ ]+method, based on traditional [ ]+ +a,c,e
concepts, but accounting for [ ]+and taking into account the +a,c,e
presence of a flaw. This analysis using faulted loading conditions enables determination of the critical flaw size. The leakage flaw is conservatively selected with a lengtn equal to [ ]+. The local stability +a,c,e
analysis is carried out by performing a [
]+of a straight piece of the accumulator line pipe containing a +a,c,e
through-wall circumferential flaw subjected to internal pressure and external loadings (faulted conditions). The objective of the local analysis is to show that unstable crack extension will not result for a flaw [
]+calculated by the global analysis. +a,c,e

The leak rate is calculated for the [ ]+ condition. [+a,c,e
]+ The crack +a,c,e
opening area resulting from [ ]+ loads is determined from an +a,c,e
assumed through-wall flaw of [ ]+ +a,c,e
[ ]+ is accounted for in determining the leak rate through this +a,c,e
crack. The leak rate is compared with the detection criterion of 1 gpm
(Reg. Guide 1.45). The leak rate prediction model is an [

]+ This method was +a,c,e
used earlier to estimate the leak rates through postulated cracks in the PWR
primary coolant loop. [1-1]

1.3 REFERENCES

+a,c,e

1-1 Palusamy, S. S. and Hartmann, A. J., "Mechanistic Fracture Evaluation of Reactor Coolant Pipe Containing a Postulated Circumferential Through-Wall Crack", WCAP-9558 Rev. 2, Class 2, June 1981, Westinghouse Nuclear Energy Systems.

2.0 FAILURE CRITERIA FOR FLAWED PIPES

2.1 GENERAL CONSIDERATIONS

Active research is being carried out in industry and universities as well as other research organizations to establish fracture criteria for ductile materials. Criteria, being investigated, include those based on J integral initiation toughness, equivalent energy, crack opening displacement, crack opening stretch, crack opening angle, net-section yield, tearing modulus and void nucleation. Several of these criteria are discussed in a recent ASTM publication [2-1].

A practical approach based on the ability to obtain material properties and to make calculations using the available tools, was used in selecting the criteria for this investigation. The ultimate objective is to show that the accumulator line containing a conservatively assumed circumferential through-wall flaw is stable under the worst combination of postulated faulted and operating condition loads within acceptable engineering accuracy. With this viewpoint, two mechanisms of failure, namely, local and global failure are considered.

2.2 GLOBAL FAILURE MECHANISM

For a tough ductile material if one assumes that the material is notch insensitive then the global failure will be governed by plastic collapse. Extensive literature is available on this subject. The recent PVRC study [2-2] reviews the literature as well as data from several tests on piping components and discusses the details of analytical methods, assumptions and methods of correlating experiments and analysis.

A schematic description of the plastic behavior and the definition of plastic load is shown in Figure 2-1. For a given geometry and loading, the plastic load is defined to be the peak load reached in a generalized load versus displacement plot and corresponds to the point of instability.

A simplified version of this criterion, namely, net section yield criterion has been successfully used in the prediction of the load carrying capacity of pipes containing gross size through-wall flaws [2-3] and was found to correlate well with experiment. This criterion can be summarized by the following relationship:

$$Wa < Wp \qquad (2\text{-}1)$$

where Wa = applied generalized load

Wp = calculated generalized plastic load

In this report, Wp will be obtained by an [

]$^{+}$ $^{+a,c,e}$

2.3 LOCAL FAILURE MECHANISM

The local mechanism of failure is primarily dominated by the crack tip behavior in terms of crack-tip blunting, initiation, extension and finally crack instability. The material properties and geometry of the pipe, flaw size, shape and loadings are parameters used in the evaluation of local failure.

The stability will be assumed if the crack does not initiate at all. It has been accepted that the initiation toughness, measured in terms of J_{IN} from a J-integral resistance curve is a material parameter defining the crack initiation. If, for a given load, the calculated J-integral value is shown to be less than J_{IN} of the material, then the crack will not initiate.

If the initiation criterion is not met, one can calculate the tearing modulus as defined by the following relation:

$$T_{app} = \frac{dJ}{da}\frac{E}{\sigma_f{}^2} \qquad (2\text{-}2)$$

where T_{app} = applied tearing modulus

E = modulus of elasticity

σ_f = flow stress = [ ]+ +a,c,e

a = crack length

[=

]+ +a,c,e

In summary, the local crack stability will be established by the two step criteria:

$$J < J_{IN}, \text{ or} \tag{2-3}$$

$$T_{app} < T_{mat}, \text{ if } J > J_{IN} \tag{2-4}$$

2.4 OPERATION AND STABILITY OF THE REACTOR COOLANT SYSTEM

The Westinghouse reactor coolant system has an operating history which demonstrates its inherent stability characteristics of the design. This includes a low susceptibility to cracking failure from the effects of corrosion (e.g., intergranular stress corrosion cracking), water hammer, or fatigue (low and high cycle). This operating history totals over 400 reactor-years, including five plants each having 15 years of operation and 15 other plants each with over 10 years of operation.

2.4.1 Stress Corrosion Cracking

For the Westinghouse plants, there is no history of cracking failure in the reactor coolant system. For stress corrosion cracking (SCC) to occur in piping, the following three conditions must exist simultaneously: high tensile stresses, a susceptible material, and a corrosive environment (Reference 2-4). Since some residual stresses and some degree of material susceptibility exist in any stainless steel piping, the potential for stress corrosion is minimized by proper material selection immune to SCC as well as preventing the occurrence of a corrosive environment. The material specifications consider compatibility with the system's operating environment (both internal and external) as well as other materials in the system, applicable ASME Code rules, fracture toughness, welding, fabrication, and processing.

The environments known to increase the susceptibilty of austenitic stainless steel to stress corrosion are (Reference 2-4): oxygen, fluorides, chlorides, hydroxides, hydrogen peroxide, and reduced forms of sulfur (e.g., sulfides, sulfites, and thionates). Strict pipe cleaning standards prior to operation and careful control of water chemistry during plant operation are used to prevent the occurrence of a corrosive environment. Prior to being put into service, the piping is cleaned internally and externally. During flushes and preoperational testing, water chemistry is controlled in accordance with written specifications. External cleaning for Class 1 stainless steel piping includes patch tests to monitor and control chloride and fluoride levels. For preoperational flushes, influent water chemistry is controlled. Requirements on chlorides, fluorides, conductivity, and pH are included in the acceptance criteria for the piping.

During plant operation, the reactor coolant water chemistry is monitored and maintained within very specific limits. Contaminant concentrations are kept below the thresholds known to be conducive to stress corrosion cracking with the major water chemistry control standards being included in the plant operating procedures as a condition for plant operation. For example, during normal power operation, oxygen concentration in the RCS is expected to be less than 0.005 ppm by controlling charging flow chemistry and maintaining hydrogen in the reactor coolant at specified considerations. Halogen concentrations are also stringently controlled by maintaining concentrations of chlorides and fluorides within the specified limits. This is assured by controlling charging flow chemistry and specifying proper wetted surface materials.

2.4.2 Water Hammer

Overall, there is a low potential for water hammer in the RCS since it is designed and operated to preclude the voiding condition in normally filled lines. The reactor coolant system, including piping and primary components, is designed for normal, upset, emergency, and faulted condition transients. The design requirements are conservative relative to both the number of transients and their severity. Relief valve actuation and the associated hydraulic transients following valve opening are considered in the system design. Other valve and pump actuations are relatively slow transients with

no significant effect on the system dynamic loads. To ensure dynamic system stability, reactor coolant parameters are stringently controlled. Temperature during normal operation is maintained within a narrow range by control rod position; pressure is controlled by pressurizer heaters and pressurizer spray also within a narrow range for steady-state conditions. The flow characteristics of the system remain constant during a fuel cycle because the only governing parameters, namely system resistance and the reactor coolant pump characteristics, are controlled in the design process. Additionally, Westinghouse has instrumented typical reactor coolant systems to verify the flow and vibration characteristics of the system. Preoperational testing and operating experience have verified the Westinghouse approach. The operating transients of the RCS are such that no significant water hammer can occur.

2.4.3 Low Cycle and High Cycle Fatigue

Low cycle fatigue considerations are accounted for in the design of the piping system through the fatigue usage factor evaluation to show compliance with the rules of Section III of the ASME Code. A further evaluation of the low cycle fatigue loadings was carried out as part of this study in the form of a fatigue crack growth analysis, as discussed in Section 8.

High cycle fatigue loads in the system would result primarily from pump vibrations during operation. During operation, an alarm signals the exceedance of the pump shaft vibration limits. Field measurements have been made on the reactor coolant loop piping of a number of plants during hot functional testing. Stresses in the elbow below the RC pump have been found to be very small, between 2 and 3 ksi at the highest. These stresses are well below the fatigue endurance limit for the material and would also result in an applied stress intensity factor below the threshold for fatigue crack growth.

Test measurements indicate that the cold leg excitation is predominantly at 20 Hz and is only .002 in. zero to peak, which is very small. The accumulator line branches from the cold leg. The fundamental mode of the Catawba accumulator line is between 6 to 8 Hz which is significantly below 20 Hz. Hence, the stresses in the accumulators line due to pump vibration will be negligible.

2.5 REFERENCES

2-1 J. D. Landes, et al., Editors, Elastic-Plastic Fracture, STP-668, ASTM, Philadelphia, PA 19109, November 1977.

2-2 J. C. Gerdeen, "A Critical Evaluation of Plastic Behavior Data and a Unified Definition of Plastic Loads for Pressure Components," Welding Research Council Bulletin No. 254.

2-3 Mechanical Fracture Predictions for Sensitized Stainless Steel Piping with Circumferential Cracks, EPRI-NP-192, September 1976.

2-4 NUREG-0691, "Investigation and Evaluation of Cracking Incidents in Piping in Pressurized Water Reactors", USNRC, September 1980.

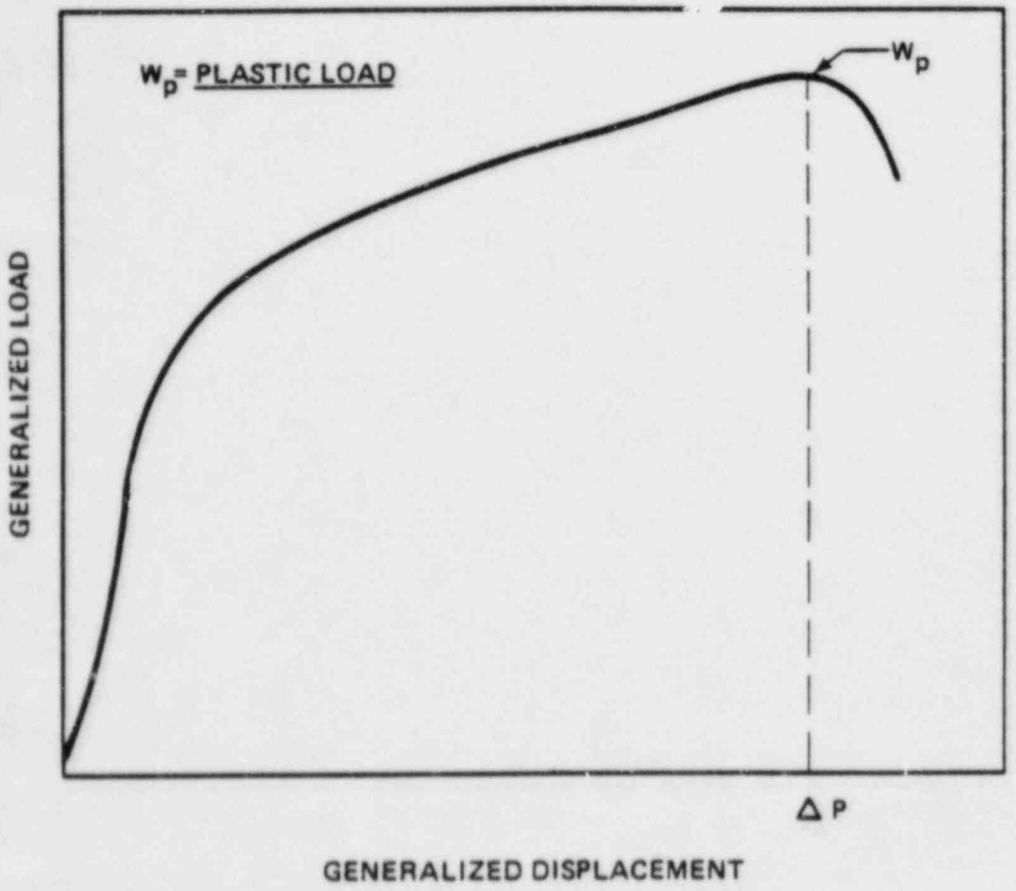

FIGURE 2-1 Schematic of Generalized Load-Deformation Behavior

3.0 LOADS FOR FRACTURE MECHANICS ANALYSIS

The accumulator line stress report [3-1] was reviewed to obtain envelope loads and materials for crack stability, leak rates and fatigue crack growth evaluations. The loads were compiled from the latest computer runs identified in [3-2], which revise the results reported in [3-1]. The envelope loads for various applications were obtained by tabulating the applicable loads at each node of all four accumulator lines of the Catawba Unit 1. The same loads are applicable to Catawba Unit 2 as it is a mirror image of Unit 1. Figure 3-1 shows a schematic layout of an accumulator line. A typical accumulator line consists of Class 1 and Class 2 portions and high and low pressure regions as shown in Figure 3-1.

The stresses due to axial loads and bending moments were calculated by the following equation:

$$\sigma = \frac{F}{A} + \frac{M}{Z} \qquad (3.1)$$

where,

σ = stress
F = axial load
M = bending moment
A = metal cross-sectional area
Z = section modulus

The bending moments for the desired loading combinations were calculated by the following equation:

$$M = \sqrt{M_Y^2 + M_Z^2} \qquad (3.2)$$

where,

M = bending moment for required loading
M_Y = Y component of bending moment
M_Z = Z component of bending moment

The axial load and bending moments for various fracture mechanics applications were computed by the methods explained in Sections 3.1, 3.2 and 3.3.

3.1 CRACK STABILITY ANALYSIS

The faulted loads for the crack stability analysis were calculated by the following equations:

$$F = |F_{DW} + F_{TH1}| + |F_{SSE}| + |F_P| \quad (3.3)$$

$$M_Y = |(M_Y)_{DW} + (M_Y)_{TH1}| + |(M_Y)_{SSE}| \quad (3.4)$$

$$M_Z = |(M_Z)_{DW} + (M_Z)_{TH1}| + |(M_Z)_{SSE}| \quad (3.5)$$

where the subscripts of the above equations represent the following loading cases,

DW = deadweight
TH1 = maximum thermal expansion including applicable thermal anchor motion
SSE = SSE loading including seismic anchor motion
P = load due to internal pressure

3.2 LEAK

The normal operating loads for leak rate predictions were calculated by the following equations:

$$F = |F_{DW} + F_{TH2} + F_p| \quad (3.6)$$

$$M_Y = |(M_Y)_{DW} + (M_Y)_{TH2}| \quad (3.7)$$

$$M_Z = |(M_Z)_{DW} + (M_Z)_{TH2}| \quad (3.8)$$

where the subscript TH2 represents normal operating thermal expansion loading including the applicable thermal anchor motion. All other parameters and subscripts are same as those explained in Section 3.1.

3.3 FATIGUE CRACK GROWTH

The normal operating loads for fatigue crack growth analysis were computed by equations 3.6, 3.7, and 3.8, i.e., the same method as that used for leak rate

loading (Section 3.2). The stresses due to normal operating loads were superimposed on through wall axial stresses due to thermal transient to obtain total stress for fatigue crack growth as explained in Section 7.6.

3.4 SUMMARY OF LOADS, GEOMETRY AND MATERIALS

Table 3-1 provides a summary of envelope loads computed for fracture mechanics evaluations in accordance with the methods explained in Sections 3.1, 3.2, and 3.3. The cross-sectional dimensions and materials are summarized in Table 3-2.

3.5 REFERENCES

3-1 EDS Report No. 03-0093-1029, Revision 0, "ASME Boiler and Pressure Vessel Code Section III Class 1 Stress Report for the Cold Leg Safety Injection System, Catawba Nuclear Station Unit No. 1."

3-2 Duke Power letter No. CN-84M-21, 2/20/84, "Catawba Nuclear Station Unit 1 Information Required for Fracture Mechanics Study."

3-3 Duke Power letter No. CN-84M-39, date 4/4/84, Subject: Catawba Nuclear Stations Unit 1 - Westinghouse "Leak Before Break" Analysis.

TABLE 3-1

CATAWBA ACCUMULATOR LINE ENVELOPE LOADS

Condition	ACCUMULATOR LINE NUMBER							
	NI04		NI05		NI06		NI07	
	F(3) (K)	M (in-K)	F (K)	M (in-K)	F (K)	M (in-K)	F (K)	M (in-K)
High Pressure Region								
- Highest Faulted(1)	[							+a,c,e]
- Corresponding Normal(2)								
Low Pressure Region								
- Highest Faulted								
- Corresponding Normal								

* From Reference 3-3

(1) Load for crack-stability

(2) Load for leak rate and fatigue crack growth

(3) Axial loads do not include internal pressure load

TABLE 3-2

ACCUMULATOR LINE GEOMETRY AND MATERIALS

Component	Pressure Region	Material	Outside Diameter D_o (in)	Wall Thickness t (in)	
Cold Leg Nozzle	High	[			+a,c,e
Pipe	High				
Fittings (Tees, Elbows)	High				
Pipe	Low				
Fittings (Tees, Elbows)	Low	]			

(a) For Catawba Unit 1
(b) For Catawba Unit 2
(c) Nominal Thickness
(d) Reduced Thickness at Weld
(e) Per ANSI B16.9

A. Critical Section for Crack Stability
and Fatigue Crack Growth

1. [+a,c,e

2.]

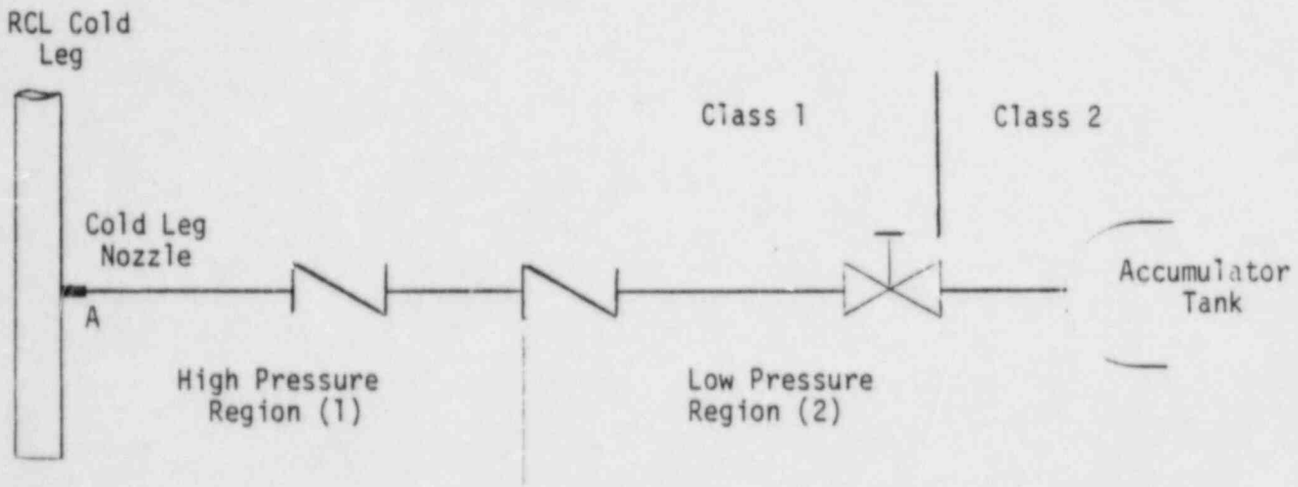

FIGURE 3-1: SCHEMATIC LAYOUT OF ACCUMULATOR LINE

4.0 CRITICAL FLAW SIZE CALCULATION

The conditions which lead to failure in stainless steel must be determined using plastic fracture methodology because of the large amount of deformation accompanying fracture. A conservative method for predicting the failure of ductile material is the [

]+ The flawed pipe is predicted to fail +a,c,e

when the [

]+ +a,c,e

This methodology has been shown to be applicable to ductile piping through a large number of experiments, and will be used here to predict the critical flaw size in the accumulator line. The failure criterion has been obtained by [

]+ The detailed development is provided in +a,c,e

Appendix A, for a through-wall circumferential flaw in a pipe with [internal pressure, axial force and imposed bending moments.]+ The [ ]+ for +a,c,e

these conditions is:

[ ]+ +a,c,e

where

[ ] +a,c,e

The analytical model described above accurately accounts for the piping internal pressure as well as imposed axial force as they affect the [ ]+ In order to validate the model, analytical predictions were compared with the experimental results [4-1] as shown in Figure 4-2. Good agreement was found. +a,c,e

In order to calculate the critical flaw size, a plot of the [ ]+ versus crack length is generated as shown in Figure 4-3. The critical flaw size corresponds to the intersection of this curve and the maximum load line. +a,c,e

The critical flaw size at the [ ] is [ ] using ASME Code [4-2] [ ] stainless steel. +a,c,e

Since [ ] for crack smaller than [ ] and [ ] the global stability criterion of Section 2.0 is satisfied. +a,c,e

Similarily, the critical flaw size in the low pressure pipe is [ ] associated with a moment of [ ] at a pipe to elbow weld. +a,c,e

An earlier calculation based on a conservative moment of [ ]+ yielded a critical flaw size of [ ].+ At that time the reference flaw was chosen as [ ]+ and consequently was used in the leak rate and local stability evaluations. +a,c,e

Reference

4-1 Kanninen, M. F., et al., "Mechanical Fracture Predictions for Sensitized Stainless Steel Piping with Circumferential Cracks" EPRI NP-192, September 1976.

4-2 ASME Section III, Division 1-Appendices, 1983 Edition, July 1, 1983.

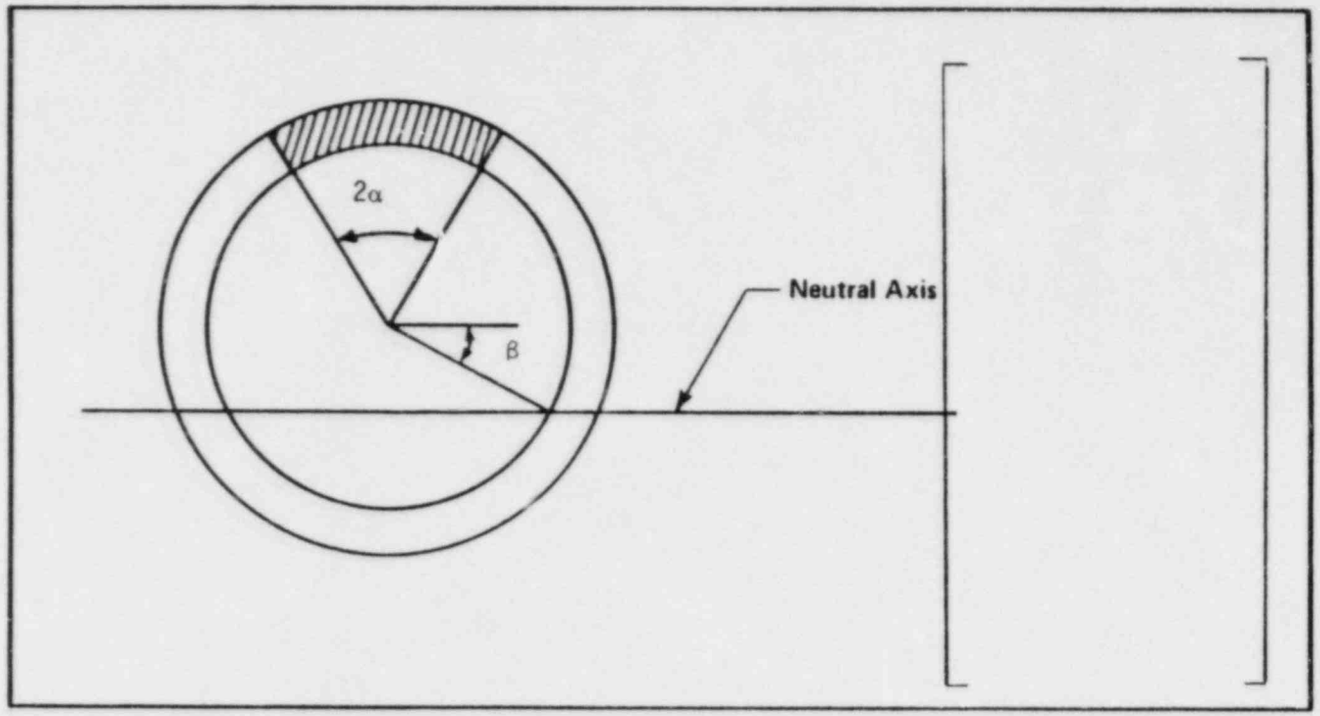

+a,c,e

FIGURE 4-1 [ ] stress distribution

+a,c,e

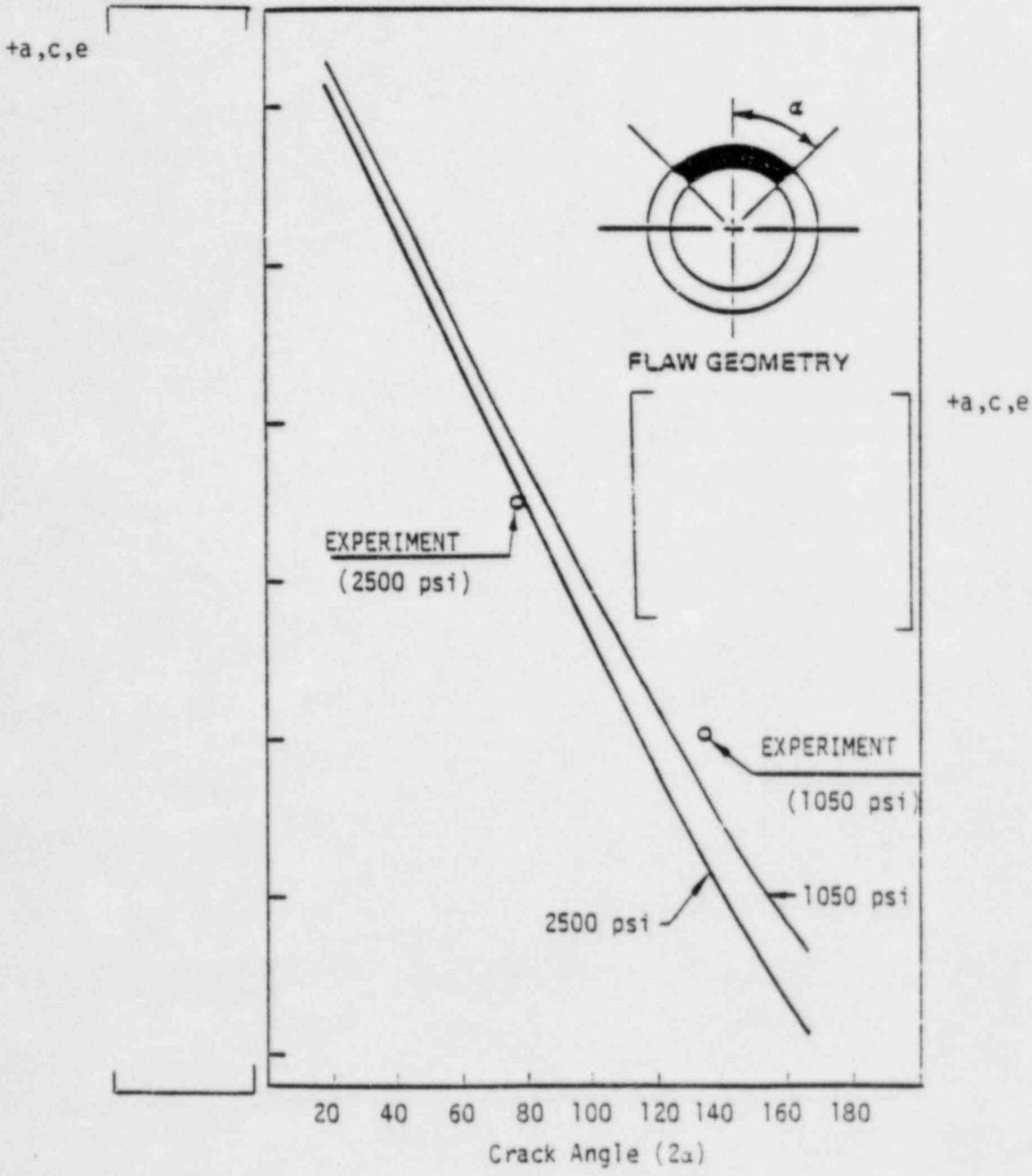

FIGURE 4-2 Comparison of[ ]predictions with Experimental +a,c,e Results

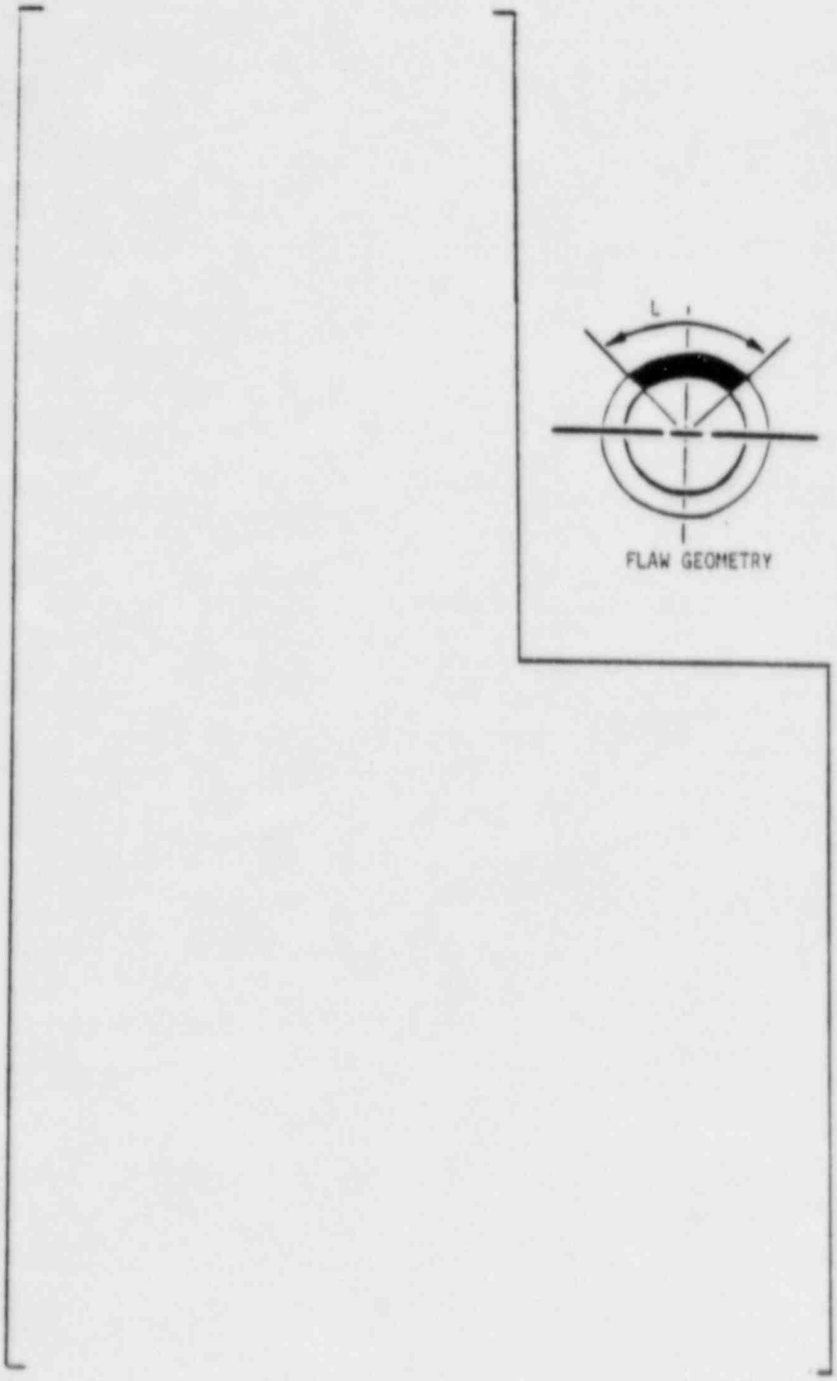

Figure 4-3 Critical Flaw Size for Accumulator Line

5.0 ANALYSIS FOR CRACK STABILITY CALCULATIONS

Using the [ ]+computer program, a [ ]+crack was analyzed to determine the local stability in the high pressure region. The loadings consists of [ ] +a,c,e +a,c,e +a,c,e

5.1 THE [ ]+MODEL AND THE MATERIAL PROPERTIES +a,c,e

Figure 5-1 identifies all the loads acting on the pipe. The pipe thickness is [ ],+ based on the thinnest location of the accumulator line under investigation. The outer diameter is [ ].+ Due to symmetry only one half of the circumference, i.e., 180-degree, is modeled. The length of the model is [ ]+which is sufficiently long to attenuate the effect of the crack for correct boundary load input from the pipe end. Figures 5-2 through 5-7 all show the [ ]+used for analysis. The [ ]+are identified in Figure 5-2 through 5-5. The [ ]+of interest for later leak rate predictions are shown in detail on Figure 5-6. The [ ]+and their Z-coordinates required for the application of the axial loads and the bending moment are shown in Figure 5-7. +a,c,e +a,c,e +a,c,e +a,c,e +a,c,e +a,c,e

[

]+ +a,c,e

The true stress-strain curve of the material is shown in Figures 5-8. The data are taken from the "Nuclear System Materials Handbook [5-2] for the stainless steel [ ]+ The stress-strain curve is [ ]+ It has been shown that the [ ]+approximation gives good agreement with the experimental results +a,c,e +a,c,e +a,c,e

[5-3]. The material properties used in the present analysis are [

]+ +a,c,e

5.2 BOUNDARY CONDITIONS AND METHOD OF LOADING

The boundary conditions are described in Figure 5-9. The pipe is subjected to the internal pressure of [ ]+and an axial load of [ ] A +a,c,e
bending moment of [ ]+is then superposed to the pipe while the +a,c,e
pressure and the axial loads are held constant. Due to non-linear material behavior, the loads are added to the pipe [
]+ +a,c,e

Figures 5-10, 5-11 and 5-12 show the sequence of applying the loads to the [ ]+model of the pipe. Figure 5-10 shows [+a,c,e

]+after which it is held steady. As shown in Figure 5-11, the axial load +a,c,e
due to [

]+ Figure 5-12 shows application of +a,c,e
the moment, starting at load step 2, where [
]+ +a,c,e

5.3 METHOD OF ANALYSIS

As mentioned in Section 2 of the present report the local instability criterion is based on the information of the [

]+ +a,c,e

[

]+ This method has been successfully used to analyze a +a,c,e
cracked pipe under a combined axial load and bending moment [5-5].

The[ ]method has been incorporated in the [ ]+a,c,e
] to calculate the average [ ]+ of a crack as well as the]+a,c,e
[ ]+along the crack front for both [ ]+a,c,e
]+analyses. The [ ]+at each load level can be computed by way]+a,c,e
of the [ ] solution strategy.]+a,c,e

5.4 [ ]+RESULTS]+a,c,e

It should be noted that [ ]+refer to two stages of a]+a,c,e
fracture process of a material. If the [
]+ Under this condition the [ ]+need]+a,c,e
not be evaluated. Figure 5-13 shows how the calculated value of the [
]+increases up to and beyond the maximum operating loading at[ ]+ +a,c,e
At the maximum loading, the [ ]+has a corresponding value of [
]+as shown on the figure. The J-value as a function of loads is]+a,c,e
shown in Table 5-1. The verification of the analysis is shown in Appen-]+a,c,e
dix B.

Since J_I at the maximum load is larger than the initiation toughness[ ]+a,c,e
][5-3]), crack extension will occur and tearing modulus T_{app}, has to be evaluated to examine the stability condition. The value of T_{app} can be calculated by the following upper bound equation proposed by Tada et. al. [5-6].

$$T_{app} = F_1(\alpha, \bar{f}) \frac{L}{R_m} + F_2(\alpha, \bar{f}) \frac{JE}{\sigma_f^2 R_m} \qquad (5\text{-}1)$$

Where

L = length of accumulator line

R_m = mean radius of pipe

α = half the angle subtended by the through-wall crack at the center of pipe cross section, (Figure 4-1)

T = pipe thickness

σ_f = flow stress

E = modulus of elasticity

β = angular location of neutral axis, (Figure 4-1)

F = the axial load on the pipe

$$\bar{f} = \frac{F}{2\pi R_m T \sigma_f} \tag{5-2}$$

$$F_1 = \frac{2}{\pi} \left(\sin \beta + \cos \alpha - \frac{\pi}{2} \bar{f} \cos \beta\right)^2 \tag{5-3}$$

$$F_2 = \frac{1}{2} \frac{(\cos \beta - 2 \sin \alpha + \frac{\pi}{2} \bar{f} \sin \beta)}{(\sin \beta + \cos \alpha - \frac{\pi}{2} \bar{f} \cos \beta)} \tag{5-4}$$

$$\beta = \frac{1}{2} \alpha + \frac{\pi}{2} \bar{f} \tag{5-5}$$

Equation (5-1) shows that T_{app} is proportional to the ratio of pipe length to radius (L/R) and the applied J-integral, J. The coefficients are functions of the geometrical and material data of the pipe. The accumulator line is composed of several pipe segments connected by elbows between the supports. The length of the longest segment may be considered as L for the stability analysis, and in line [ ] feet. The data needed for +a,c,e computing T_{app} are listed below by using Equations (5-1) through (5-5):

R_m = [ ] +a,c,e

t = [ ]

α = [ ]

$2a$ = [ ]

σ_f = [ ]

F = [ ]

$\bar{f}$ = [ ]

β = [ ]

F_1 = [ ]

F_2 = [ ]

L = [ ]

J = [ ]

E = [ ]

Substituting these data in Equation (5-1), one obtains T_{app} = [ ] +a,c,e

5.5 STABILITY EVALUATION FOR CRACK IN BASE METAL

J-R curves for [ ] stainless steel specimens corresponding to the minimum +a,c,e J_{IN} and T_{mat} are shown in Figures 5-14 and 5-15, respectively [5-3]. It should be noted that one specimen was tested up to a load corresponding to a [ ] This data is judged to +a,c,e be applicable to a slightly lower temperature [ ] in the region analyzed. +a,c,e Thus, we have the following condition:

$$T_{app} < T_{mat}$$

It is therefore concluded that the[ ]long through-wall circumferential flaw in the most severe region of the accumulator line will not become unstable locally to cause a double ended rupture. +a,c,e

The above analysis was repeated assuming a [ ] reference flaw which is greater than 1/2 the critical flaw size as defined by the moment of [ ]. Results gave a $T_{applied}$ of [ ] again assuring local stability. +a,c,e +a,c,e

5.6 STABILITY EVALUATION FOR A CRACK IN THE PIPE WELD

The axial stress σ_A resulting from the applied axial load is given by:

$$\sigma_A = \frac{P}{2\pi Rt} = [\quad]\text{psi} \qquad +a,c,e$$

where

$P = [\quad]$ +a,c,e

$R = [\quad]$

$t = [\quad]$

The bending stress caused by the applied moment is:

$$\sigma_B = \frac{M}{\pi R^2 t} = [\quad]\text{psi} \qquad +a,c,e$$

where

M = bending moment,[ ]in-lb. +a,c,e

The total of these two stresses ($\sigma_A + \sigma_B$) is[ ]psi, which is well below the minimum yield stress[ ]obtained from test results reported in Reference 5-7. For this reason, linear elastic fracture mechanics methods are applicable for calculating the applied stress intensity factor and its corresponding [ ]. +a,c,e +a,c,e +a,c,e

Appendix B of this report has equations for computing the stress intensity factors due to axial load and the stress intensity factors due to bending. Using these equations

$$K_{Ia} = 1.109\ \sigma_A\ \sqrt{\pi a} \qquad \text{(for axial load)}$$

$$K_{Ib} = 1.076\ \sigma_B\ \sqrt{\pi a} \qquad \text{(for bending)}$$

where

a = one half of the total crack length,[ ] +a,c,e

Substituting the numerical values for σ_A, σ_B, and a, we find:

K_{Ia} =[ ]+ psi√in and K_{Ib} =[ ]+ psi√in +a,c,e

Adding these together, a total applied stress intensity factor (K) of[ ] +a,c,e psi√in is obtained. Using this value, plastic zone correction for K is made by first calculating the "effective crack length", a_{eff}:

$$a_{eff} = a + r_p = a + \frac{1}{2\pi} \cdot \frac{K^2}{\sigma_y^2} = [\quad]+ \qquad +a,c,e$$

The stress intensity factor is then increased by the factor

$\sqrt{a_{eff}/a}$ =[ ] to give the corrected K (or K_p): +a,c,e

K_p =[ ] psi√in +a,c,e

The applied J integral will be as follows:

$$J_{app} = \frac{K_p^2}{E} = \left[\quad\right] \frac{\text{in-lbs}}{\text{in}^2} \qquad +a,c,e$$

This value of J_{app} is substantially less than J_{Ic} for the worst case[ ]reported in Reference 5-8. +a,c,e

In this reference, the weld material is shown to be less limiting than the worst case [ ] under plant operating temperatures. Also for low temperature +a,c,e conditions on the low pressure side, J_{Ic} for welds are reported to be around [ ] +a,c,e in-lb/in^2. Much higher values for J_{Ic} are reported in References 5-3 and 5-7. Thus local stability is assured.

5.7 LOW PRESSURE REGION

A similar calculation was made for the low pressure region assuming the presence of [5.1 inch] reference flaw. The calculated J_{app} was [ ]. thus assuring +a,c,e local stability since per reference 5-8, room temperature J_{Ic} values for weld metal are reported at [ ]. +a,c,e

5.8 REFERENCES

5-1 Klaus-Jurgen Bathe, "ADINA, A Finite Element Program for Automatic Dynamic Incremental Nonlinear Analysis," 1978, MIT Report 83448-1.

5-2 Nuclear System Materials Handbook, Volume I Design Data, Revision 1, 10/1/76.

5-3 Palusamy, S. S., Hartmann, A. J., "Mechanistic Fracture Evaluation of Reactor Coolant Pipe Containing a Postulated Circumferential Through Wall Crack," WCAP 9558, Revision 2, dated May 1982.

5-4 Parks, D. M., "The Virtual Crack Extension Method for Nonlinear Material Behavior," Computer Methods in Applied Mechanics and Engineering," Vol. 12, 1977, pp. 353-364.

5-5 Yang, C. Y. and S. S. Palusamy, "VCE Method of J Determination for a Pressurized Pipe Under Bending," J. of Pressure Vessel Technology, Trans. ASME, Vol. 105, 1983, pp. 16-22.

5-6 Tada, H.; P. C. Paris, and R. M. Gamble, "A Stability Analysis of Circumferential Cracks for Reactor Piping Systems", in Fracture Mechanics, ASTM STP 700, 1980, pp 296-313.

5-7 Palusamy, S. S., Tensile and Toughness Properties of Primary Piping Weld Metal for use in Mechanistic Fracture Evaluation, WCAP 9787, May 1981.

5-8 Bamford, W. H., et. al., The Effect of Thermal Aging on the Structural Integrity of Cast Stainless Steel Piping for Westinghouse Nuclear Steam Supply Systems, WCAP-10456, Westinghouse Proprietary Class 2, November 1983.

TABLE 5-1 J_I VERSUS THE APPLIED LOADS. CIRCUMFERENTIAL CRACK

[ ] +a,c,e

SOLUTION STEP	AXIAL STRESS (KSI)	BENDING MOMENT (IN-KIP)	J_I (IN-LB/IN^2)
1	[		] +a,c,e
2			
3			
4			
5			
6			
7			
8			
9			
10			
11			
12			
13			
14			
15	]		]

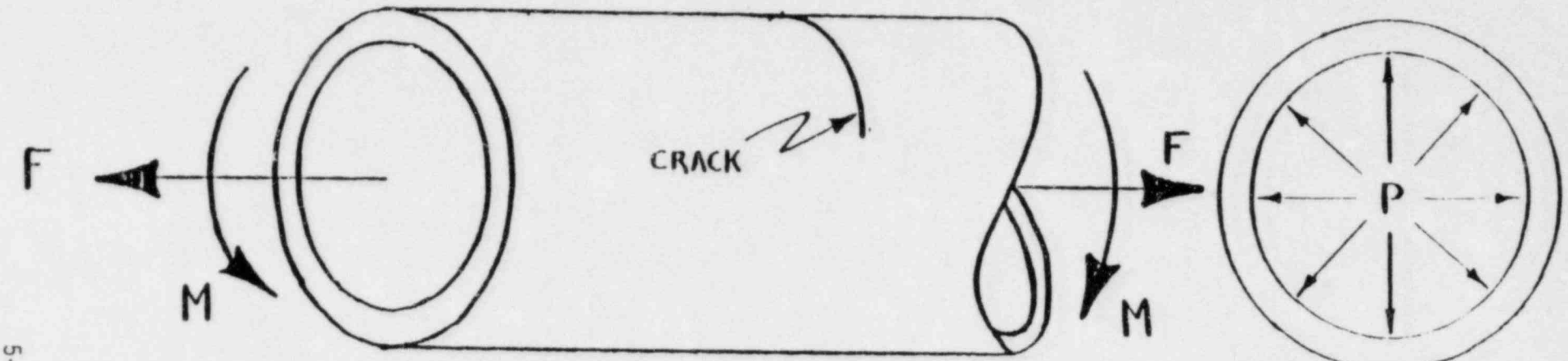

+a,c,e

[ ]

FIGURE 5-1 LOADS ACTING ON THE PIPE

+a,

[

+a,c,e

]

+a,c,e

Figure 5-2 [

]

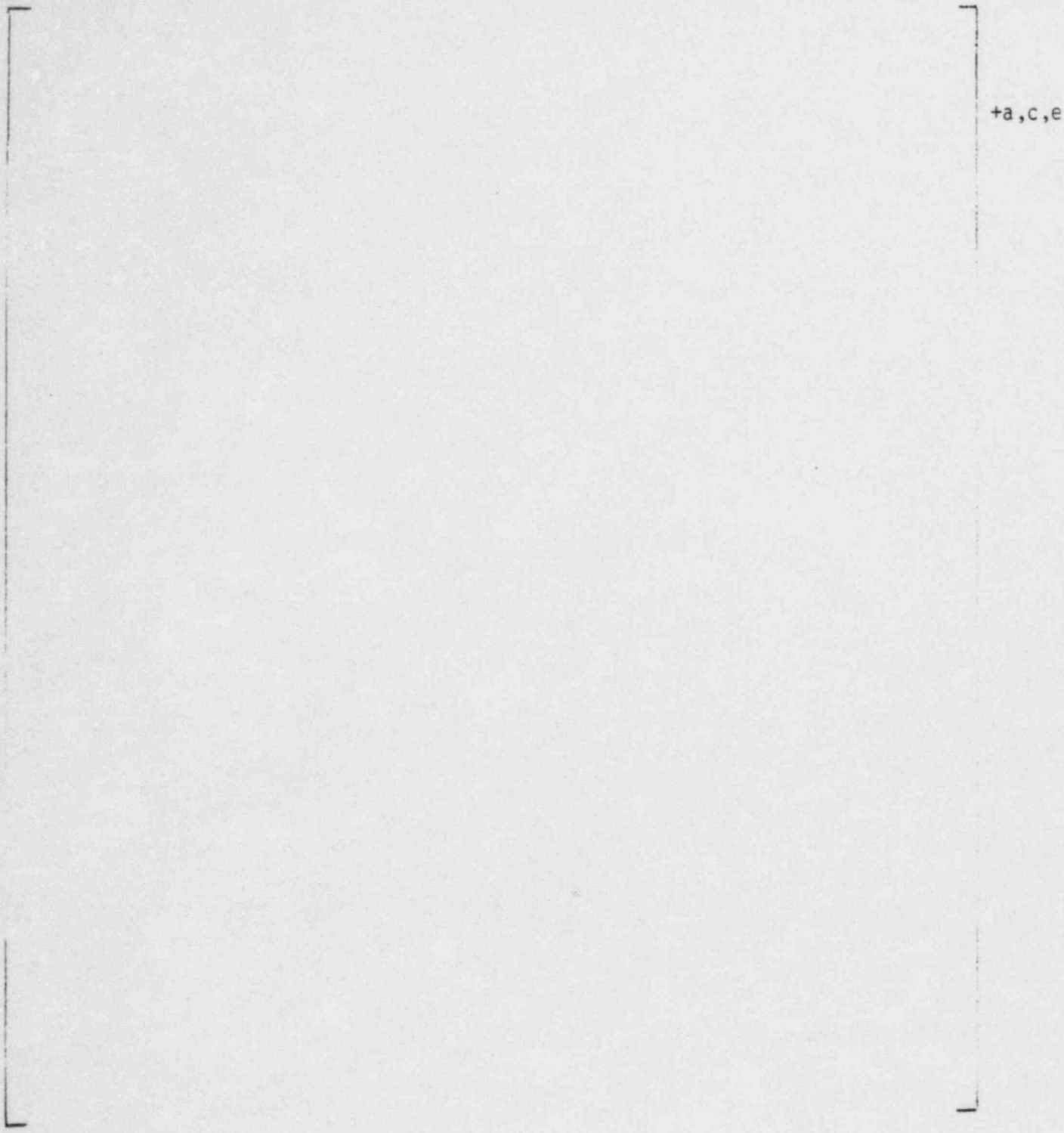

+a,c,e

+a,c,e

Figure 5-3 [

]

+a,c,e

[

]

+a,c,e

Figure 5-4 [

]

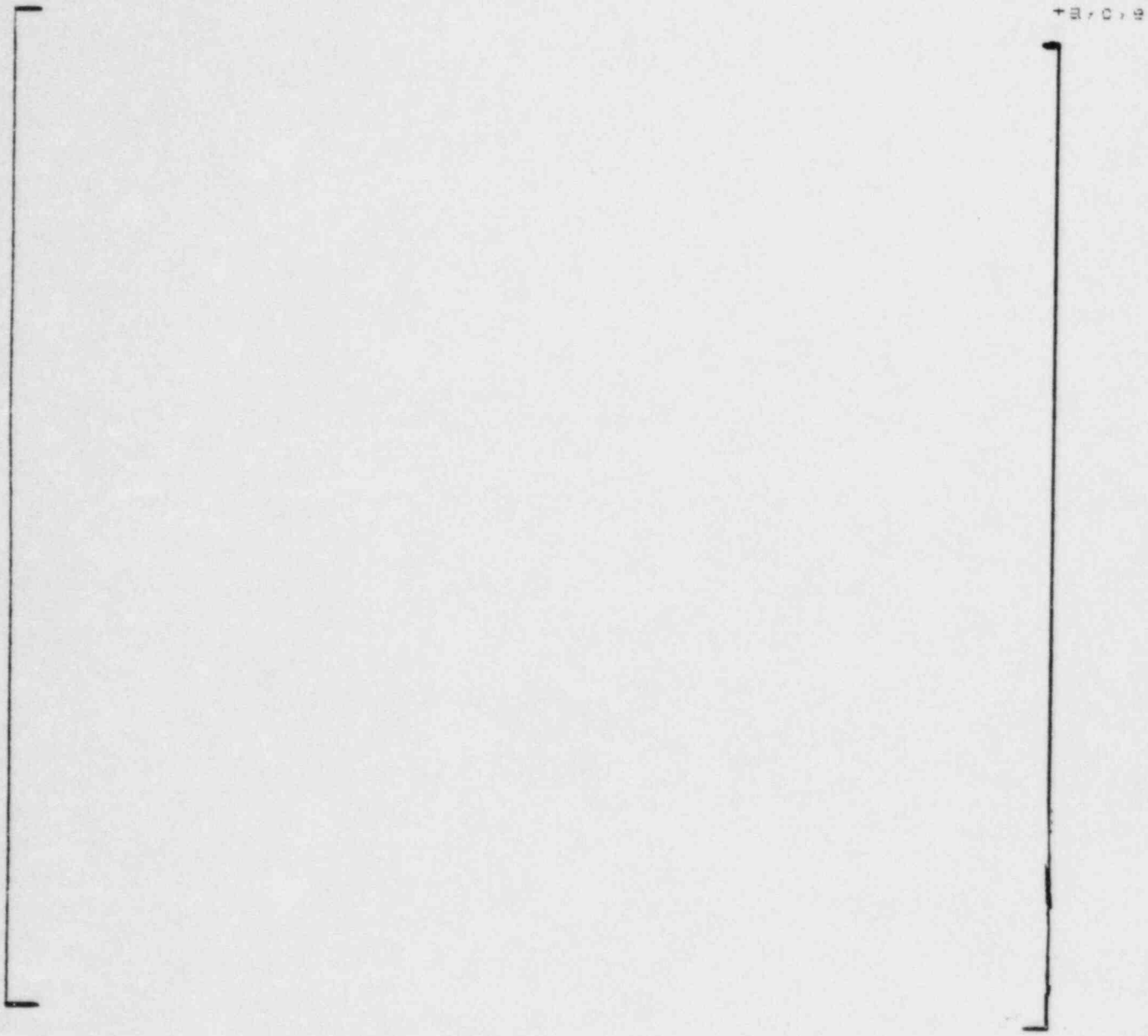

FIGURE 5-5 The [ ] pattern in the vicinity of the crack front. +a,c,e

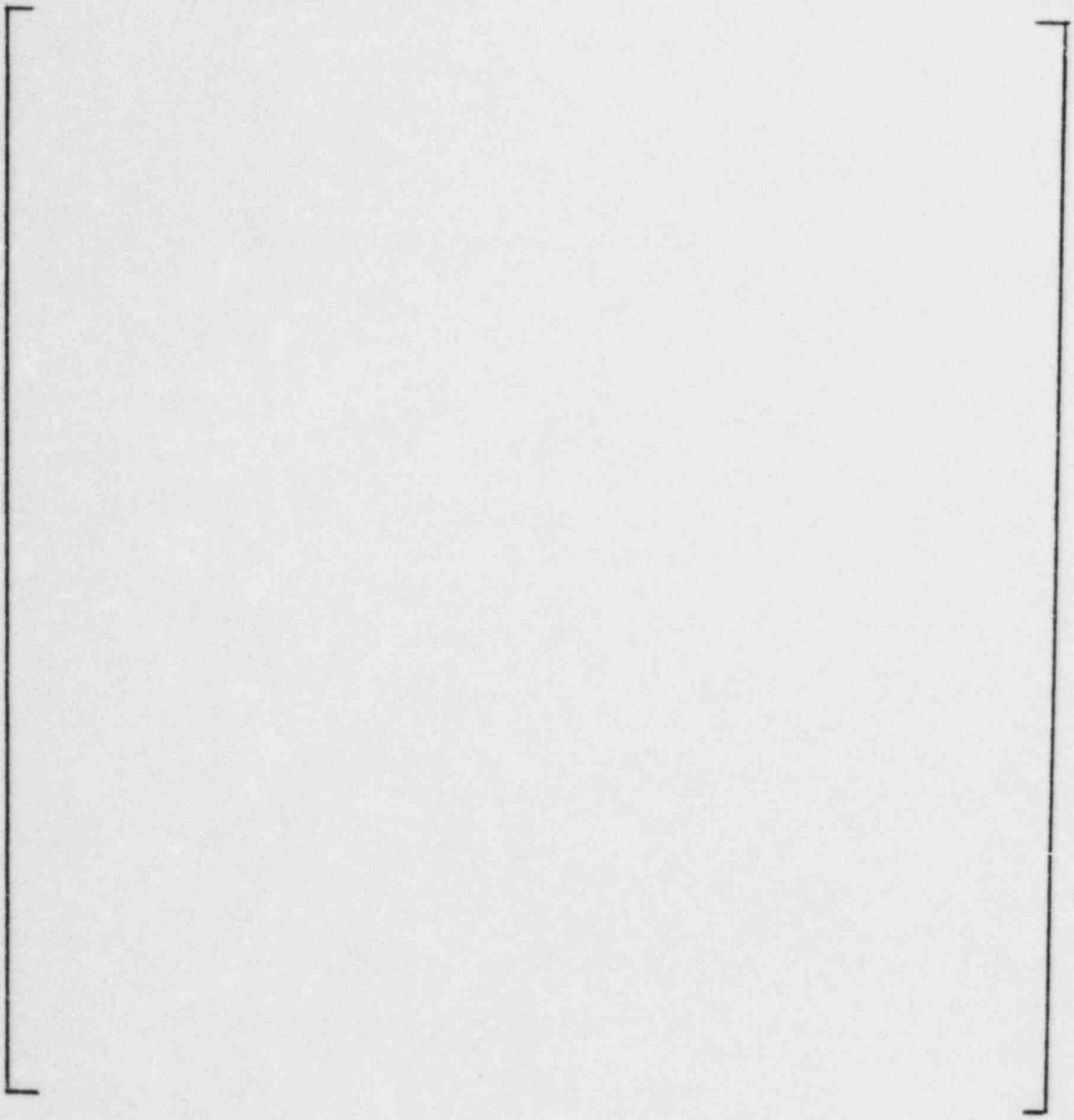

+a,c,e

Figure 5-6 [ ]on the middle of the crack surface +a,c,e

Figure 5-7 [ ]and their z-coordinates at the pipe end which +a,c,e
is subjected to the applied axial and bending loads

STRESS-STRAIN CURVE.[ ] +a,c,e

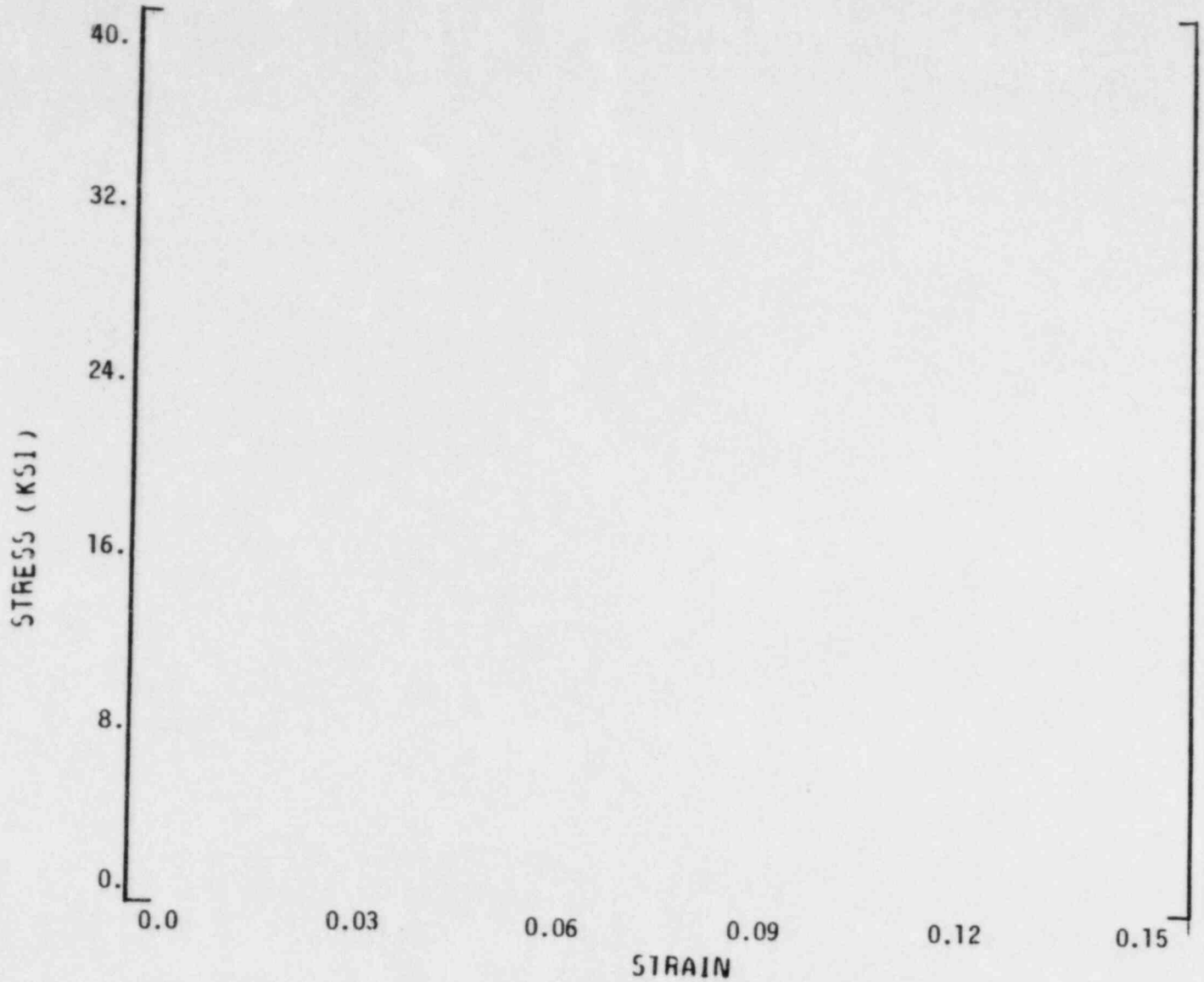

+a,c,e

Figure 5-8 [ ]Stress-Strain curve and[ ] +a,c,e

Figure 5-9 Schematic of the boundary conditions.

Figure 5-10 Loading schedule for the internal pressure applied to the inside surface of the pipe

Figure 5-11 Loading schedule for the uniform axial stress (including pressure) applied to the pipe end

Figure 5-12 Loading schedule for the bending moment applied to the pipe end

J VS. M (CATAWBA ACCUMULATOR LINE)

[

+a,c,e

J (IN-KIP/IN^2)

]

Figure 5-13 [

]

+a,c,e

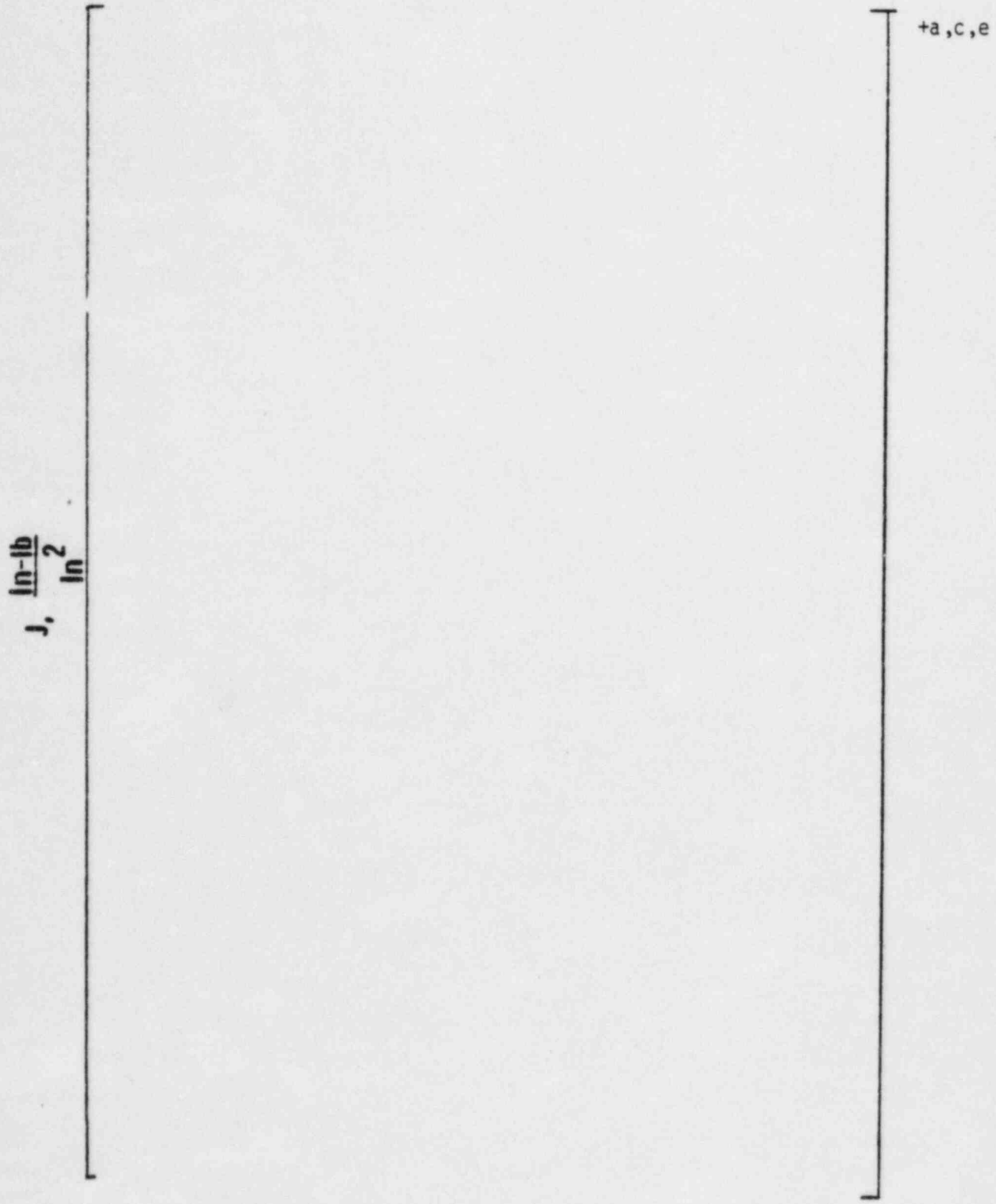

FIGURE 5-14 JR-curve for[ ] +a,c,e

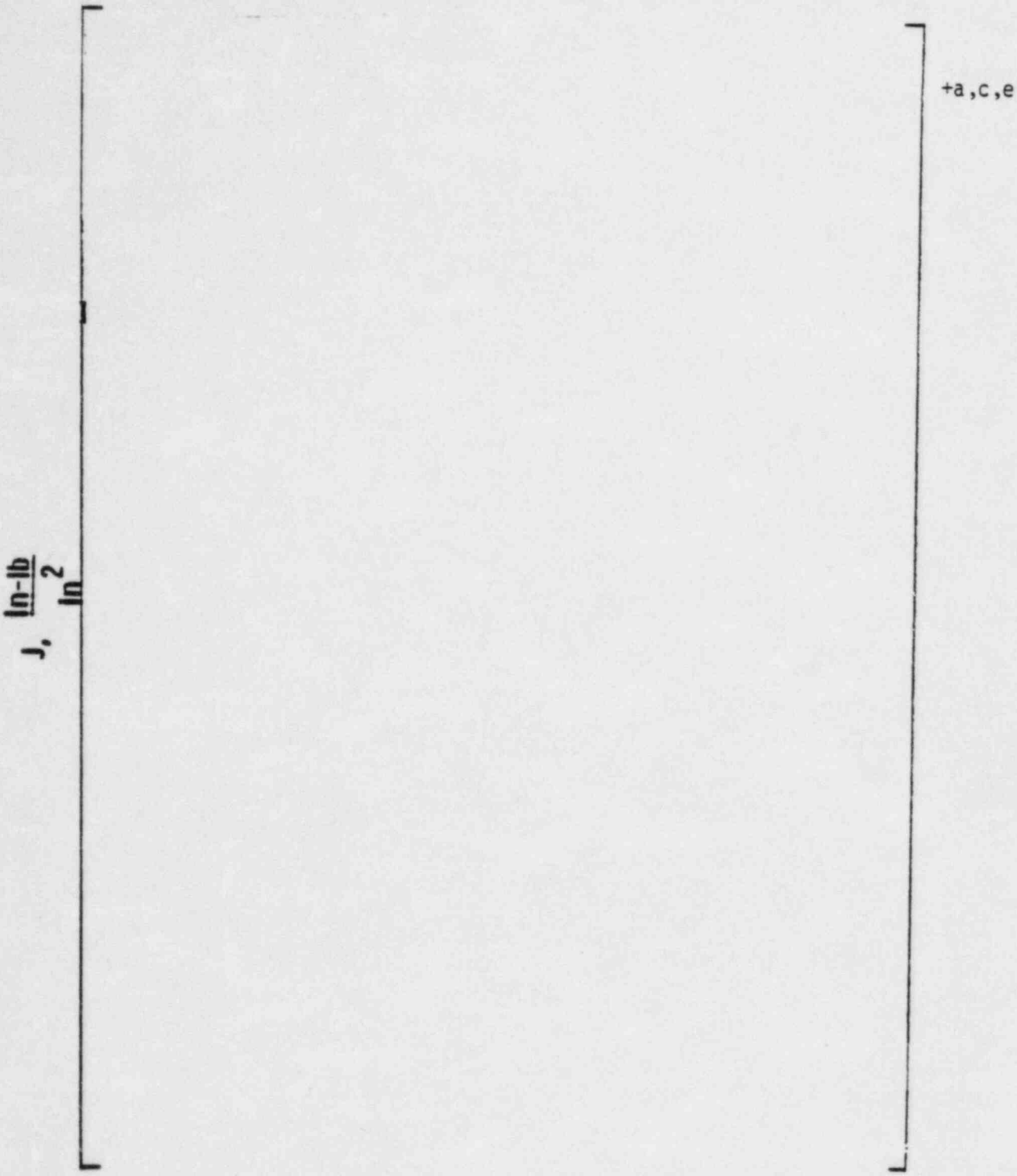

FIGURE 5-15 JR-curve for [ ] +a,c,e

6.0 LEAK RATE PREDICTIONS

6.1 INTRODUCTION

Detailed fracture mechanics analysis has shown that through-wall cracks in the accumulator line would remain stable and not cause a gross failure of this RCS component. If such a through-wall crack did exist, it would be desirable to detect the leakage such that the plant could be brought to a safe shutdown condition. The purpose of this section is to discuss the method which will be used to predict the flow through such postulated cracks and present the leak rate calculation results for [+a,c,e
] long through wall circumferential cracks using the [ ] +a,c,e
method. The mechanical stability of the cracks has been shown in Section 5.0.

6.2 GENERAL CONSIDERATIONS

The flow of hot accumulator water through an opening to a lower back pressure causes flashing which can result in choking. For long channels where the ratio of the channel length, L, to hydraulic diameter, D_H, (L/D_H) is greater than [ ],† both [ ] must be considered. +a,c,e
In this situation the flow can be described as being single phase through the channel until the local pressure equals the saturation pressure of the fluid. At this point, the flow beings to flash and choking occurs. Pressure losses due to momentum changes will dominate for [ ] However, for large +a,c,e
L/D_H values, friction pressure drop will become important and must be considered along with the momentum losses due to flashing.

6.3 CALCULATION METHOD

The basic method used in the leak rate calculations is the method developed by [+a,c,e

]

The flow rate through a crack was calculated in the following manner. Figure 6-1 from [ ]+ was used to estimate the critical pressure, Pc, for the accumulator line enthalpy condition and an assumed flow. Once Pc was found for a given mass flow, the [ ]+ was found from Figure 6-2 of [ ] For all cases considered, since [ ]+ [ ]+ Therefore, this method will yield the two-phase pressure drop due to momentum effects as illustrated in Figure 6-3. Now using the assumed flow rate G, the frictional pressure drop can be calculated using +a,c,e +a,c,e +a,c,e +a,c,e

$$\Delta P_f = [\quad]^+ \qquad (6\text{-}1)$$ +a,c,e

where the friction factor f is determined using the [ ]+ The crack relative roughness, ε, was obtained from fatigue crack data on stainless steel samples. The relative roughness value used in these calculations was [ ]+RMS as taken from Reference [6-3]. +a,c,e +a,c,e

The frictional pressure drop using Equation (6-1) is then calculated for the assumed flow and added to the [ ]+ to obtain the total pressure drop from the primary system to the atmosphere. That is +a,c,e

$$\text{Accumulator Line Pressure} - 14.7 = [\quad]^+ \qquad (6\text{-}2)$$ +a,c,e

for a given assumed flow G. If the right-hand-side of Equation (6-2) does not agree with the pressure difference between the accumulator line and atmosphere, then the procedure is repeated until Equation (6-2) is satisfied to within an acceptable tolerance and this then results in the flow value through the crack. This calculational procedure has been recommended by [ ]+ for this type of [ ]+ calculation. The leak rates obtained by this method have been compared in Reference [ ]+ with experimental results. The comparison indicated that the method predicts leak rate with acceptable accuracy [ ].+ +a,c,e +a,c,e +a,c,e +a,c,e

For the low pressure region, both the fluid temperature and the temperature outside the pipe are at ambient condition. Thus, the flow is at a constant temperature condition and from a high pressure region to a low pressure region. Therefore, the leak rate for this case is obtained by[ ]given in references 6-4 and 6-5. The pressure drop due to friction is included in predicting the leak rate. The leak rate Q is given by the following equation: a,c,e

$$Q = \sqrt{\frac{2g\Delta p}{k\rho}}\, A \qquad (6\text{-}3)$$

where Δp is a pressure difference between stagnation and back pressure, g is the acceleration of gravity, ρ is the density at atmospheric condition and k is associated with a friction coefficient (k) given by $k = (f)\,(L/D_h) + 1.5$, and A is the crack opening area.

6.4 CRACK OPENING AREAS

Figure 6-4 shows the shape of one quarter of the opened crack at the mean radius of the pipe, when the pressure and axial loadings reach their full values of [ ], respectively. Figure 6-5 is a similar plot when a moment of [ ] is superposed upon it. Table 6-1 presents the coordinates and displacements of the [ ] used to generate the two figures. The area under each curve is evaluated by numerical integration. Multiplying each of the areas by 4 gives the total areas of the cracks at the mean radius of the pipe, for the two loading conditions. Two leak rates will be calculated based on these areas. These are: a,c,e +a,c,e +a,c,e

(a) Load A: the leak rate for the loading condition for the high pressure side of the accumulator where there is [ ] +a,c,e

(b) Load B: the leak rate for the loading condition where there is [ ] +a,c,e

For load A, the crack area is:

A_A = [ ] +a,c,e

For load B, the crack area is:

A_B = [ ] +a,c,e

For the low pressure side of the accumulator, where the internal pressure is[ ]crack opening areas were calculated for two cases: +a,c,e

Load C: crack opening area due to[+a,c,e

Load D: crack opening area due to[ ] +a,c,e

For load C, the crack area is:

A_c =[ ] +a,c,e

For load D, crack area is

A_d =['] +a,c,e

6.5 LEAK RATE RESULTS

6.5.1 High Pressure Side of the Accumulator [ ] +a,c,e

Using the [ ] method gives [ ] leak rate for Load Case A +a,c,e
[ ] For Load Case B, the method gives [+a,c,e
] +a,c,e

Case B is considered more realistic since it [
] Both calculated leak rates are higher than the +a,c,e
leak detection criterion of 1 gpm (Regulatory Guide 1.45).

6.5.2 Low Pressure Side of the Accumulator [ ] +a,c,e

The leak rates for cases C and D were obtained by using equation (6-3). The leak rate for case C is found to be[ ]and that for case D is obtained as [+a,c,e]at room conditions. Case D is considered more realistic since it[+a,c,e] The calculated leak rate for case D +a,c,e is higher than the leak detection criterion of 1 gpm (Regulatory Guide 1.45).

6.6 References

6-1[+a,c,e

]

6-2[+a,c,e

]

6-3 Palusamy, S. S. and Hartmann, A. J. "Mechanistic Fracture Evaluation of Reactor Coolant Pipe Containing a Postulated Circumferential Through-wall Crack," WCAP 9570 Rev. 2, Class 3, Westinghouse Nuclear Energy Systems, June 1981.

6-4 CRANE-Appendix A, Physical Properties of Fluids and Flow Characteristics of Valves, Fitting and Pipe, PA-26.

6-5 Handbook of Hydraulic - Resistance Coefficients of Local Resistance and of Friction, p. 61, AEC-TR-6630.

TABLE 6-1 CRACK SURFACE DISPLACEMENT DATA

Node Number	Arc Length from Symm. Plane (in.)	Displacement (in.) x 10^{-3} Load A	Load B
[	[		]

+a,c,e

NOTES:

1. The crack surface displacement is one half of the crack opening displacement (COD).
2. Load A: [ ] +a,c,e
3. Load B: Load A plus M = 357 in-kips.
4. [ ]locations are shown in Figure 5-6. +a,c,e

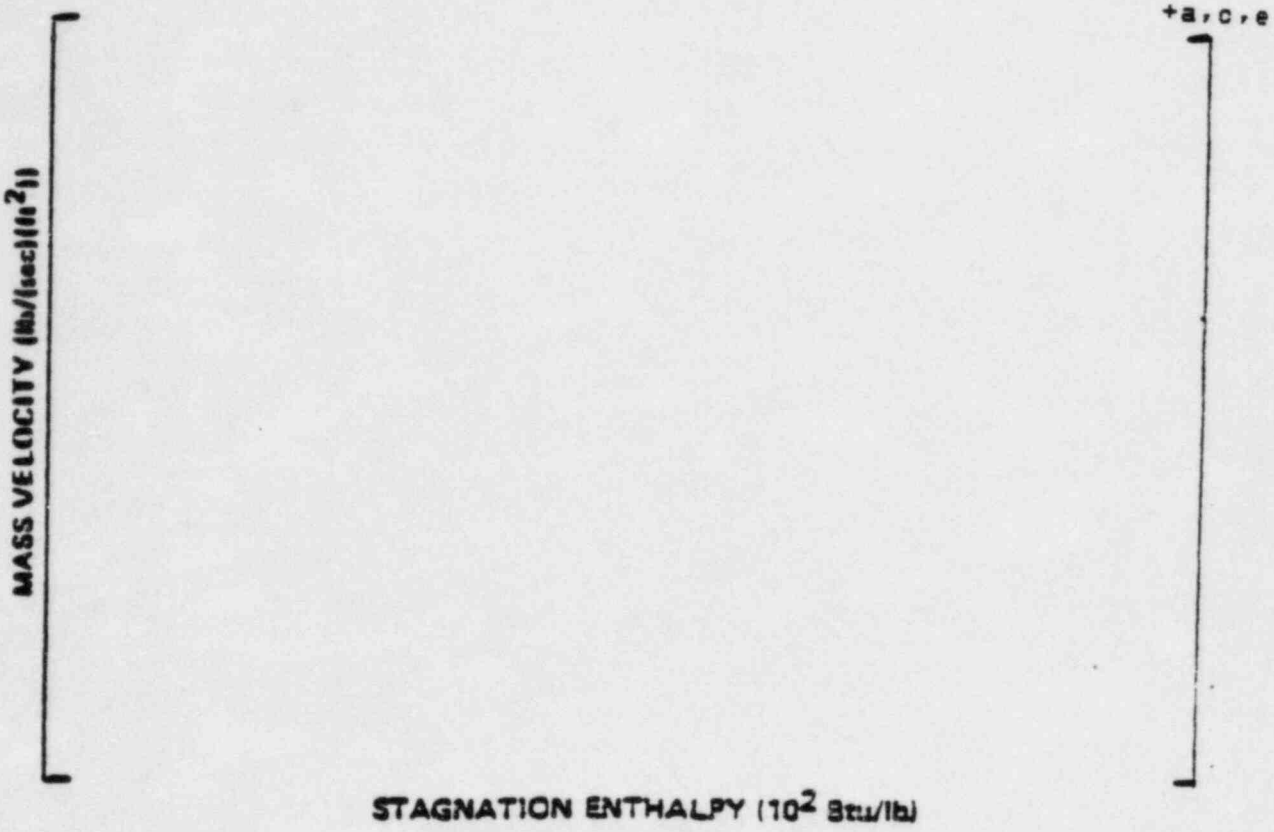

Figure 6-1 Analytical Predictions of Critical Flow Rates of Steam-Water Mixtures

+a,c,e

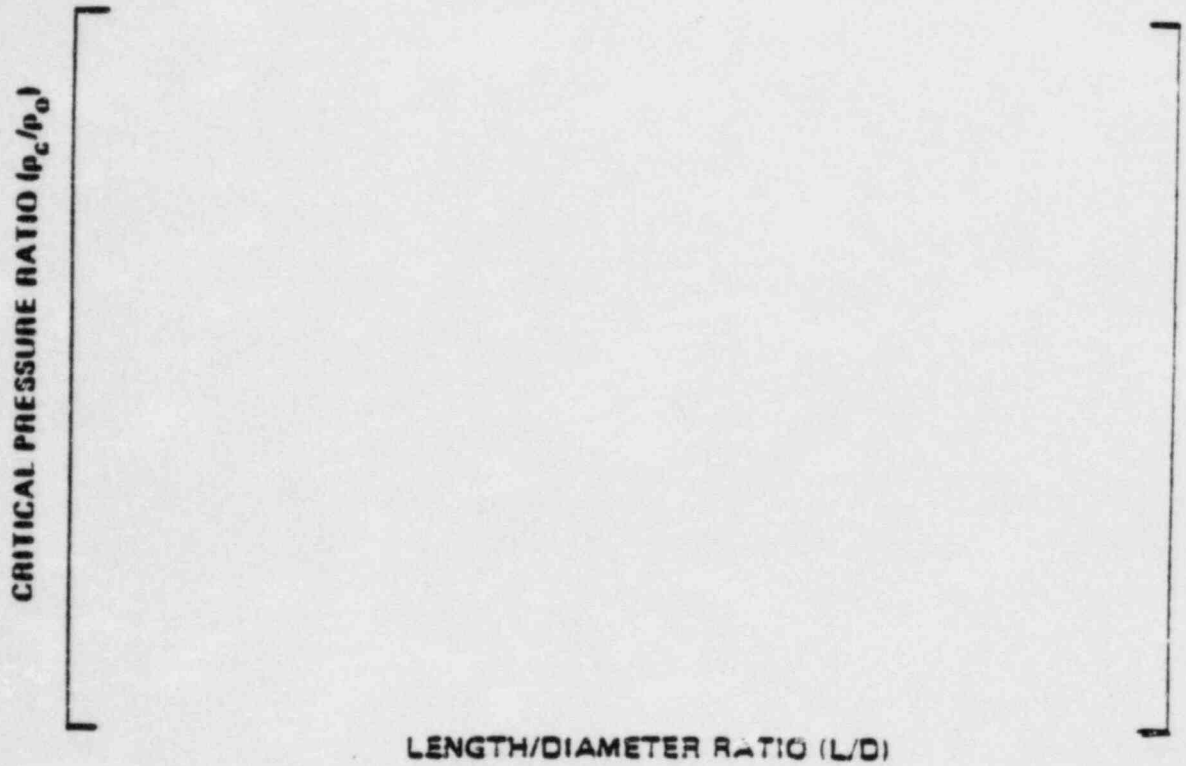

Figure 6-2 [ ] Pressure Ratio as a Function +a,c,e of L/D

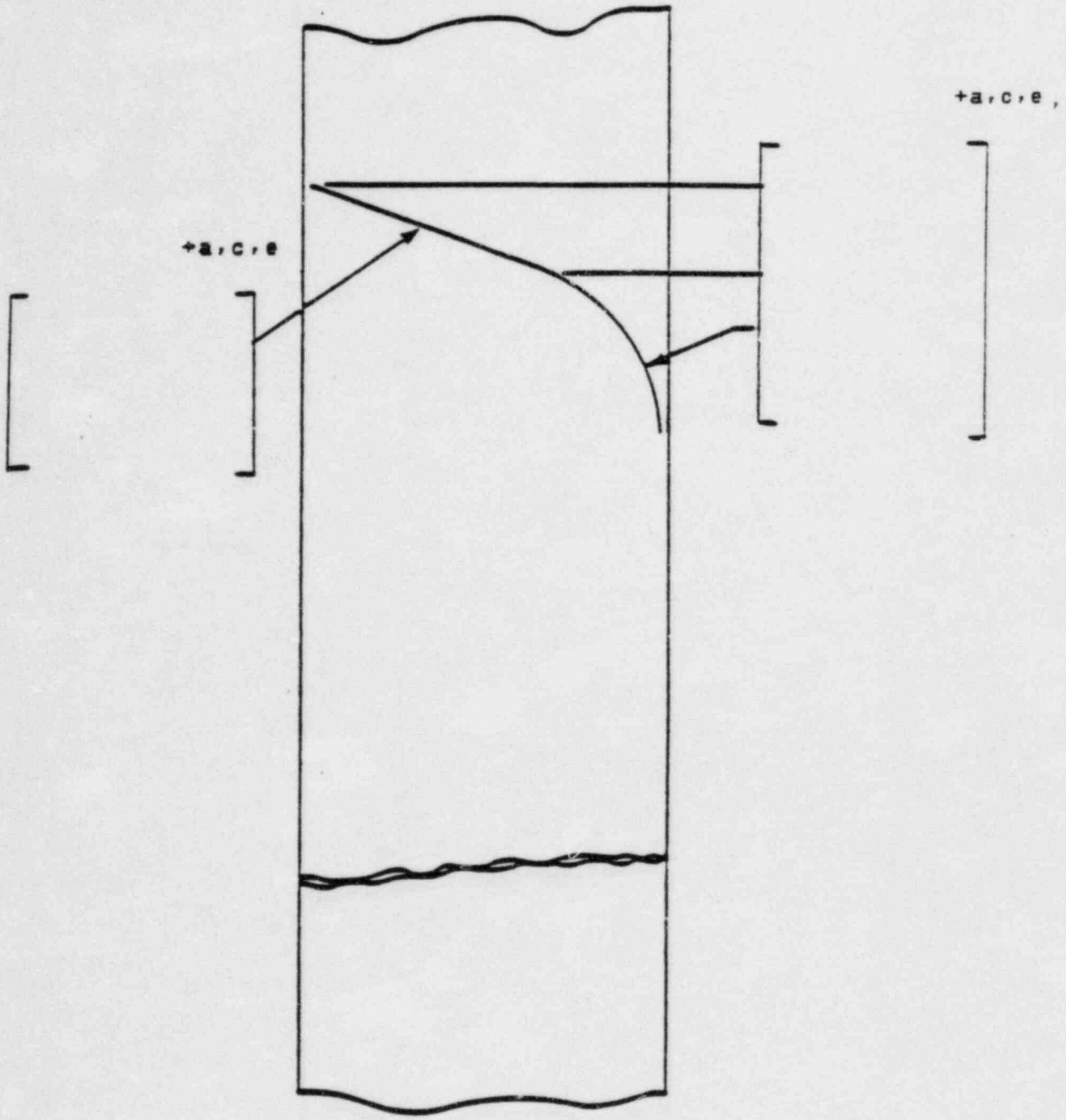

Figure 6-3 Idealized Pressure Drop Profile Through a Postulated Crack

+a,c,e

CRACK SURFACE DISPLACEMENT (INCHES)

+a,c,e

Figure 6-4 Crack surface profile under[ ]

+a,c,e

CRACK SURFACE DISPLACEMENT (INCHES)

+a,c,e

Figure 6-5 Crack surface profile under combined[

]

7.0 THERMAL TRANSIENT STRESS ANALYSIS

The thermal transient stress analysis was performed to obtain the through wall stress profiles for use in the fatigue crack growth analysis of Section 8.0. The through wall stress distribution for each transient was calculated for i) the time corresponding to the maximum inside surface stress and, ii) the time corresponding to the minimum inside surface stress. These two stress profiles are called the maximum and minimum through wall stress distribution, respectively for convenience. The constant stresses due to pressure, deadweight and thermal expansion (at normal operating temperature, [ ] a,c,e loadings were superimposed on the through wall cyclical stresses to obtain the total maximum and minimum stress profile for each transient. Linear through wall stress distributions were calculated by conservative simplified methods for all minor transients. More accurate nonlinear through wall stress distributions were developed for severe transients by finite element analysis.

7.1 CRITICAL LOCATION FOR FATIGUE CRACK GROWTH ANALYSIS

The accumulator line stress report [3-1], design thermal transients (Section 7.2), 1-D analysis data on accumulator line thermal transient stresses (based on ASME Section III NB3600 rules) and the geometry were reviewed to select the worst location for the fatigue crack growth analysis. The[ ]was +a,c,e determined to be the most critical location for the fatigue crack growth evaluation. This location is selected as the worst location (same as determined in Table 3-1) based on the following considerations:

i) the fatigue usage factor is highest.
ii) the stress due to thermal expansion is high.
iii) the effect of discontinuity due to undercut at weld will tend to increase the cyclical thermal transient loads.
iv) the review of data shows that the 1-D thermal transient stresses in the accumulator line piping section are generally higher near the[ ] +a,c,e

7.2 DESIGN TRANSIENTS

The transient conditions selected for this evaluation are based on conservative estimates of the magnitude and the frequency of the temperature fluctuations resulting from various operating conditions in the plant. These are representative of the conditions which are considered to occur during plant operation. The fatigue evaluation based on these transients provides confidence that the component is appropriate for its application over the design life of the plant. All the normal operating and upset thermal transients, in accordance with design specification [7-1] and the applicable system design criteria document [7-2], were considered for this evaluation. Out of these, 15 transients were used in the final fatigue crack growth analysis as listed in Table 7-1. These transients were selected on the basis of the following criteria:

[ ] (7.1) +a,c,e

(7.2)

where,

[ ] +a,c,e

7.3 SIMPLIFIED STRESS ANALYSIS

The simplified analysis method was used to develop conservative maximum and minimum linear through wall stress distributions due to thermal transients. In this method, a 1-D computer program was used to perform the thermal analysis to determine the through wall temperature gradients as a function of time. The inside surface stress was calculated by the following equation which is similar to the transient portion of ASME Section III NB3600, Eq. 11:

S_i = [ ] (7.3) +a,c,e

where,

S_i = inside surface stress

[(7.4) +a,c,e

(7.5)

(7.6)]

The effect of discontinuity (3rd term of Eq. 7.3) was included in the analysis by performing separate 1-D thermal analysis for the pipe and nozzle, i.e., sections a and b, respectively. The maximum and minimum inside surface stresses were searched from the S_i values calculated for each time step of the transient solution.

The outside surface stresses corresponding to maximum and minimum inside stresses were calculated by the following equations:

S_{01} = [ ] (7.7) +a,c,e

S_{02} = [ ] (7.8) +a,c,e

where,

S_{01} = outside surface stress at time t_{max}

S_{02} = outside surface stress at time t_{min}

[ ] +a,c,e

All other parameters are as defined previously

The material properties for the accumulator pipe [ ] and the RCL +a,c,e
[ ] were taken from the ASME Section III +a,c,e
1983 appendices [7-3] at the normal operating temperature [ ] of the +a,c,e
accumulator line. The values of E and α, at the normal operating temperature, provide a conservative estimation of the through wall thermal transient stresses as compared to room temperature properties. The following values were conservatively used, which represent the highest of the [+a,c,e
] materials:

E = [ ] +a,c,e
α =
ν =

The maximum and minimum linear through wall stress distribution for each thermal transient was obtained by joining the corresponding inside and outside surface stresses by a straight line. The simplified analysis discussed in this section was performed for all minor thermal transients of Table 7-1 (1 through 9, 13 and 15). Nonlinear through wall stress profiles were developed for the remaining severe transients as explained in Section 7.4. The inside and outside surface stresses calculated by simplified methods for the minor transients are shown in Table 7-2. The comparison of the through wall stress profile, computed for a typical transient by the simplified method and that based on the detailed finite element analysis, is shown in Figure 7-1. This figure shows that the simplified method provides more conservative crack growth.

7.4 STRESS DISTRIBUTION FOR SEVERE TRANSIENTS

The nonlinear stress distributions were developed for the severe transients, i.e., transient 10, 11, 12 and 14. As mentioned earlier, the accumulator line section near the [ ] is the worst location for fatigue +a,c,e crack growth analysis. A schematic of the accumulator line geometry at this location, based on [7-4, 7-5], is shown in Figure 7-2. The WECAN [7-6] 1-D axisymmetric finite element model of the accumulator piping was used for this analysis. This model was developed by using three 2-D isoparametric elements through the wall thickness with twelve nodes per element. The cross-sectional dimensions corresponding to reduced thickness, as shown for the critical section in Figure 7-2 were used in this model. This simplified model computes nonlinear through wall stress distribution but does not include the effect of discontinuity. The effect of discontinuity at the critical section (Figure 7-2) was included by increasing the magnitude of 1-D nonlinear through wall stress by 20 percent at the inside one third thickness of the pipe wall. This amplification is based on a previous transient analysis of a RCS nozzle utilizing both a detailed model of the complete nozzle and attached pipe and a simplified model as described above. Identical transients were run using both models. Comparison of the results shows that for the inside four nodes the average ratio of detailed model stress to simplified model stress is 1.12, or a 12 percent increase in stress due to the discontinuity. An increase factor of 20% was therefore conservatively chosen. The through wall stress profiles developed for the severe transients by this method are shown in Figures 7-3 through 7-6 for transients 10, 11, 12 and 14, respectively.

7.5 OBE LOADS

The stresses due to OBE loads were neglected in the fatigue crack growth analysis since these loads will not contribute significantly to crack growth due to small number of cycles.

7.6 TOTAL STRESS FOR FATIGUE CRACK GROWTH

The total through wall stress at a section was obtained by superimposing the pressure load stresses and the stresses due to deadweight and thermal expansion (normal operating case) on the thermal transient stresses (of Table 7-2 or the nonlinear stress distributions discussed in Section 7.4). Thus, the total stress for fatigue crack growth at any point is given by the following equation:

Total for Fatigue Crack Growth	=	Thermal Transient	+	Stress Due to DW + Thermal Expansion	+	Stress Due to Internal Pressure	(7.9)

The envelope thermal expansion, deadweight and pressure loads for calculating the total stresses of Equation (7.9) are summarized in Table 3-1 of Section 3.4.

7.7 REFERENCES

7-1 Duke Power Company Specification No. CNS-1206.02-01-000, Rev. 11, 11/22/1983, "Catawba Nuclear Station Units 1 & 2, Design Specification ASME Section III Class 1 Piping."

7-2 Westinghouse System Standard Design Criteria 1.3, "Nuclear Steam Supply System Design Transients," Revision 2, April 15, 1974.

7-3 ASME Section III, Division 1-Appendices, 1983 Edition, July 1, 1983.

7-4 Duke Drawing No. CN-1676-1 Rev. 3, Piping Layout Welding End Preparations.

7-5 Southwest Fabricating and Welding Co. Drawing, "ASME Section III Class 1 Butt Welding Nozzles, Rev. 3."

7-6 WECAN - Westinghouse Electric Computer Analysis, User's Manual - Volumes I, II, III and IV, Westinghouse R&D Center, Pittsburgh, PA, Third Edition, 1982.

TABLE 7-1

THERMAL TRANSIENTS CONSIDERED FOR FATIGUE CRACK GROWTH EVALUATION

Trans. No.	Description	No. of Occurrences
1		+a,c,e
2		
3		
4		
5		
6		
7		
8		
9		
10		
11		
12		
13		
14		
15		

TABLE 7-2

STRESSES FOR THE MINOR TRANSIENTS (PSI)

TRANSIENT NO.	NO. OF CYCLES	MAXIMUM INSIDE STRESS	CORRESPONDING OUTSIDE STRESS	MINIMUM INSIDE STRESS	CORRESPONDING OUTSIDE STRESS
1	[				] +a,c,e
2					
3					
4					
5					
6					
7					
8					
9					
13					
15	]				

+a,c,e

FIGURE 7-1: COMPARISON OF TYPICAL MAXIMUM AND MINIMUM STRESS PROFILE COMPUTED BY SIMPLIFIED[ ] +a,c,e

1. [ ] +a,c,e
2. [ ]

[ ] +a,c,e

FIGURE 7-2: SCHEMATIC OF ACCUMULATOR LINE AT[ ] +a,c,e

+a,c,e

FIGURE 7-3: [ ]MAXIMUM AND MINIMUM STRESS PROFILE FOR TRANSIENT #10 +a,c,e

+a,c,e

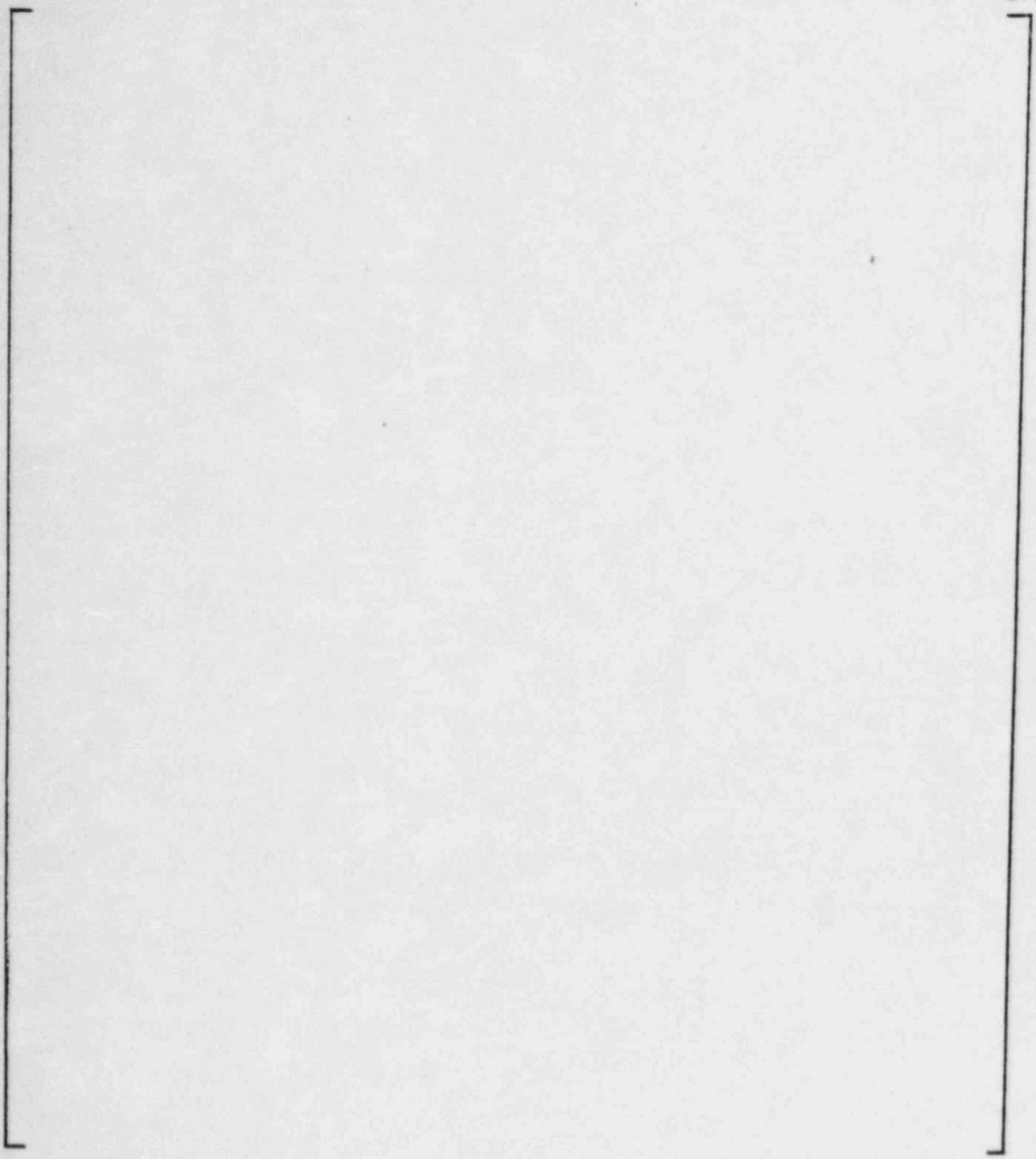

FIGURE 7-4: [ ]MAXIMUM AND MINIMUM STRESS PROFILE FOR TRANSIENT #11 +a,c,e

+a,c,e

FIGURE 7-5: [ ]MAXIMUM AND MINIMUM STRESS PROFILE FOR TRANSIENT #12 +a,c,e

+a,c,e

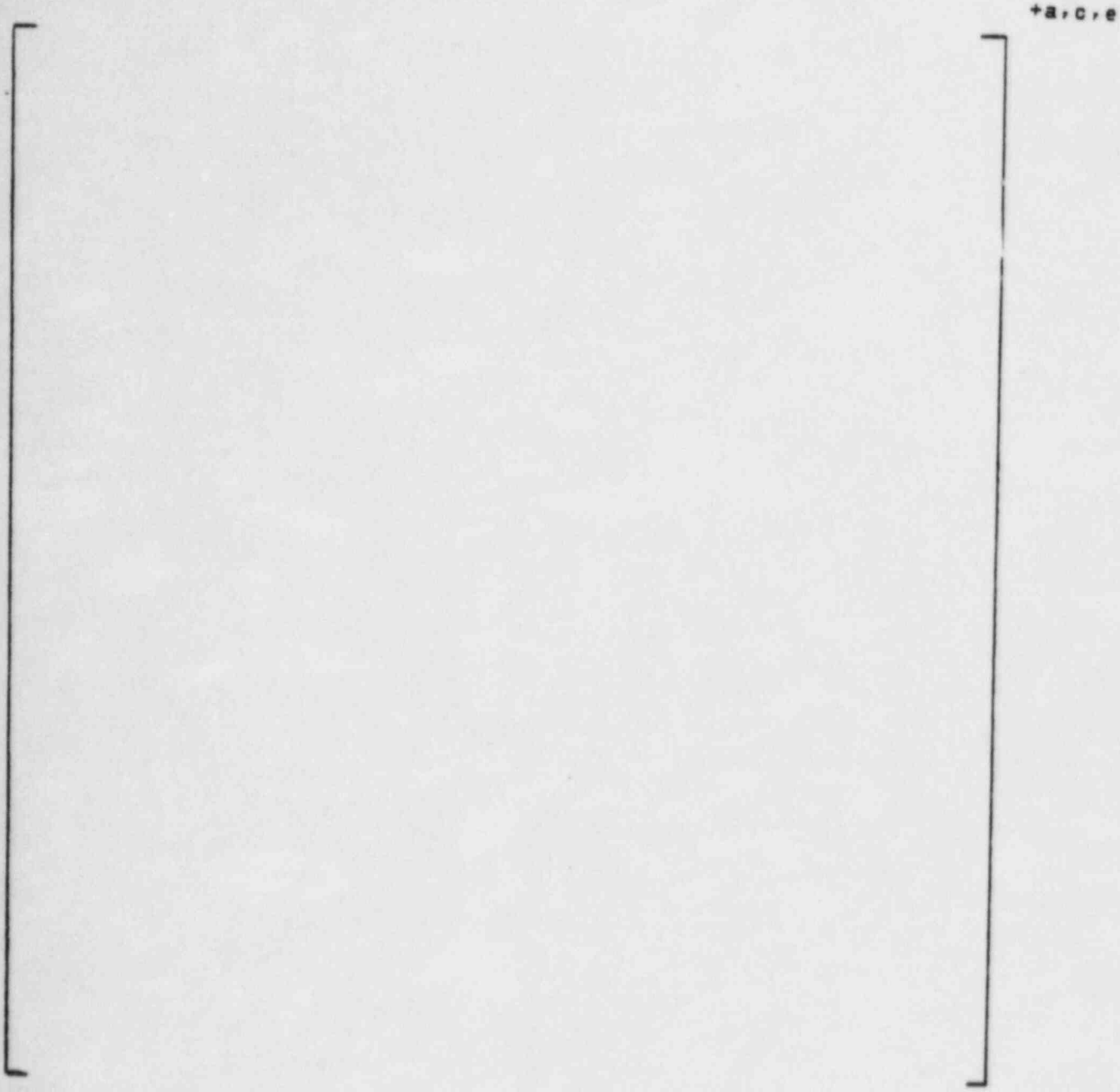

FIGURE 7-6: [ ]MAXIMUM AND MINIMUM STRESS PROFILES FOR TRANSIENT #14 +a,c,e

8.0 FATIGUE CRACK GROWTH ANALYSIS

The fatigue crack growth analysis was performed to determine the effect of the design thermal transients, in Table 7-1. The analysis was performed for the critical cross section of the model which is identified in Figure 7-2. A range of crack depths was postulated, and each was subjected to the transients in Table 7-1.

8.1 ANALYSIS PROCEDURE

The fatigue crack growth analyses presented herein were conducted in the same manner as suggested by Section XI, Appendix A of the ASME Boiler and Pressure Vessel Code. The analysis procedure involves assuming an initial flaw exists at some point and predicting the growth of that flaw due to an imposed series of stress transients. The growth of a crack per loading cycle is dependent on the range of applied stress intensity factor ΔK_I, by the following relation:

$$\frac{da}{dN} = C_o \Delta K_I^{\,n} \qquad (8.1)$$

where "Co" and the exponent "n" are material properties, and ΔK_I is defined later, in Equation (8-3). For inert environments these material properties are constants, but for some water environments they are dependent on the level of mean stress present during the cycle. This can be accounted for by adjusting the value of "Co" and "n" by a function of the ratio of minimum to maximum stress for any given transient, as will be discussed later. Fatigue crack growth properties of stainless steel in a pressurized water environment have been used in the analysis.

The input required for a fatigue crack growth analysis is basically the information necessary to calculate the parameter ΔK_I, which depends on crack and structure geometry and the range of applied stresses in the area where the crack exists. Once ΔK_I is calculated, the growth due to that particular cycle can be calculated by Equation (8-1). This increment of growth is then added to the original crack size, the ΔK_I adjusted, and the

analysis proceeds to the next transient. The procedure is continued in this manner until all the transients have been analyzed.

The crack tip stress intensity factors (K_I) to be used in the crack growth analysis were calculated using an expression which applies for a semi-elliptic surface flaw in a cylindrical geometry [8-1].

The stress intensity factor expression was taken from Reference 8-1 and was calculated using the actual stress profiles at the critical section. The maximum and minimum stress profiles corresponding to each transient were input, and each profile was fit by a third order polynomial:

$$\sigma(x) = A_0 + A_1 \frac{x}{t} + A_2 \left(\frac{x}{t}\right)^2 + A_3 \left(\frac{x}{t}\right)^3 \qquad (8\text{-}2)$$

The stress intensity factor $K_I(\phi)$ was calculated at the deepest point of the crack using the following expression:

$$K_I(\phi) = \left[\right] \qquad (8\text{-}3)$$

+a,c,e

where ϕ = angular location along crack (ϕ = 0 is deepest point of crack)

H_0, H_1, H_2, H_3 are magnification factors obtained from Reference 8-1

A_0, A_1, A_2, A_3 are coefficients from the fit of Equation (8-2)

t = section thickness

a = crack depth

$Q^{1/2}$ elliptic integral of second kind, $Q^{1/2} = \int_0^{\pi/2} (\cos^2 \phi + a^2/c^2 \sin^2\phi)^{1/2} d\phi$

c = half crack length

Calculation of the fatigue crack growth for each cycle was then carried out using the reference fatigue crack growth rate law determined from

consideration of the available data for stainless steel in a pressurized water environment. This law allows for the effect of mean stress or R ratio (K_{Imin}/K_{Imax}) on the growth rates.

The reference crack growth law for stainless steel in a pressurized water environment was taken from a collection of data [8-2] since no code curve is available, and it is defined by the following equation:

$$\frac{da}{dN} = [\quad] \qquad (8\text{-}4) \qquad +a,c,e$$

where $K_{eff} = (K_{Imax})\ (1-R)^{1/2}$

$$R = \frac{K_{Imin}}{K_{Imax}}$$

$\frac{da}{dN}$ = crack growth rate in micro-inches/cycle

8.2 RESULTS

Fatigue crack growth analyses were carried out for the critical cross section. Analysis was completed for a range of postulated flaw sizes oriented circumferentially, and the results are presented in Table 8-1. The postulated flaws are assumed to be six times as long as they are deep. Even for the largest postulated flaw of [ ]the result shows that the flaw growth through the wall will not occur during the 40 year design life of the plant. For smaller flaws, the flaw growth is significantly lower. For example, a postulated [ ] inch deep flaw will grow to [ ] which is less than [ ] the wall thickness. These results also confirm operating plant experience. There have been no leaks observed in Westinghouse PWR accumulator lines in over 400 reactor years of operation. +a,c,e +a,c,e

8.3 REFERENCES

8-1 McGowan, J. J. and Raymund, M., "Stress Intensity Factor Solutions for Internal Longitudinal Semi-Elliptical Surface Flaws in a Cylinder Under Arbitrary Loadings", Fracture Mechanics ASTM STP 677, 1979, pp. 365-380.

8-2 Bamford, W. H., "Fatigue Crack Growth of Stainless Steel Reactor Coolant Piping in a Pressurized Water Reactor Environment", ASME Trans. Journal of Pressure Vessel Technology, February 1979.

TABLE 8-1 ACCUMULATOR LINE FATIGUE CRACK GROWTH RESULTS

Wall Thickness =[ ] +a,c,e

INITIAL CRACK LENGTH (IN.)	CRACK LENGTH AFTER YEAR 10	20	30	40
[				] +a,c,e

9.0 SUMMARY AND CONCLUSIONS

A mechanistic fracture evaluation of the class 1 accumulator lines in the Catawba Unit 1 and Unit 2 plants was performed. The most limiting region for both the high pressure and low pressure segments was chosen to cover all accumulator lines in both plants.

The most limiting region in the high pressure segment is at the [ ] and that for the low pressure segment is [ ] +a,c,e +a,c,e

Corrosion, high and low cycle fatigue and water hammer were evaluated and shown either not to exist or not to cause excessive crack growth or leakage of the pressure boundary.

Thru-wall flaws were postulated to exist in both base (wrought) and weld regions of the stainless steel accumulator lines.

Postulated thru-wall, circumferential oriented flaws of 1/2 the "critical" flaw sizes as determined by limit moment were chosen as reference flaws for leak rate estimates. The reference flaw sizes were [ ] inch and [ ] inch for the high and low pressure segments, respectively. [ ] analysis was used to evaluate flaw stability by calculation of the J-integral corresponding to maximum applied load including safe-shut down earthquake loads. The J results were then used to calculate the tearing modulus, $T_{applied}$. +a,c,e +a,c,e

The T value for the [ ] inch flaw in the high pressure region and T_{mat} were [ ] and [ ], respectively for wrought material. For the weld in this region, the applied J was [ ] with J_{Ic} > [ ]. In the low pressure region the maximum calculated J value was [ ]. +a,c,e +a,c,e +a,c,e +a,c,e

Consequently, reference flaws in the high pressure region [ ] inch and low pressure [ ] inch are both locally and globally stable.

The leak rates for the reference flaw under normal operating loads were determined to be [ ] for the high pressure segment and [ ] for the low pressure segment, yielding a factor of >3 relative to the criteria of Regulatory Guide 1.45. +a,c,e

Based on the above, it is concluded that large breaks in the accumulator lines should not be considered as a part of the structural design basis for the Catawba Unit 1 and 2 plants.

APPENDIX A

EQUILIBRIUM OF THE SECTION

APPENDIX A

The internal stress system at the crack plane has to be in equilibrium with the applied loading i.e. the hydrostatic pressure P, axial force F and the bending moment M_b. The angle β which identifies the point of stress inversion follows from the equilibrium of horizontal forces (See Figure A-1). This is

[ ] +a,c,e

Solving for β,

[ ] +a,c,e

The external bending moment at the instant of failure follows from the equilibrium of moments, which is most easily taken around the axis 1-1. Thus M_b can be determined from

[ ] +a,c,e

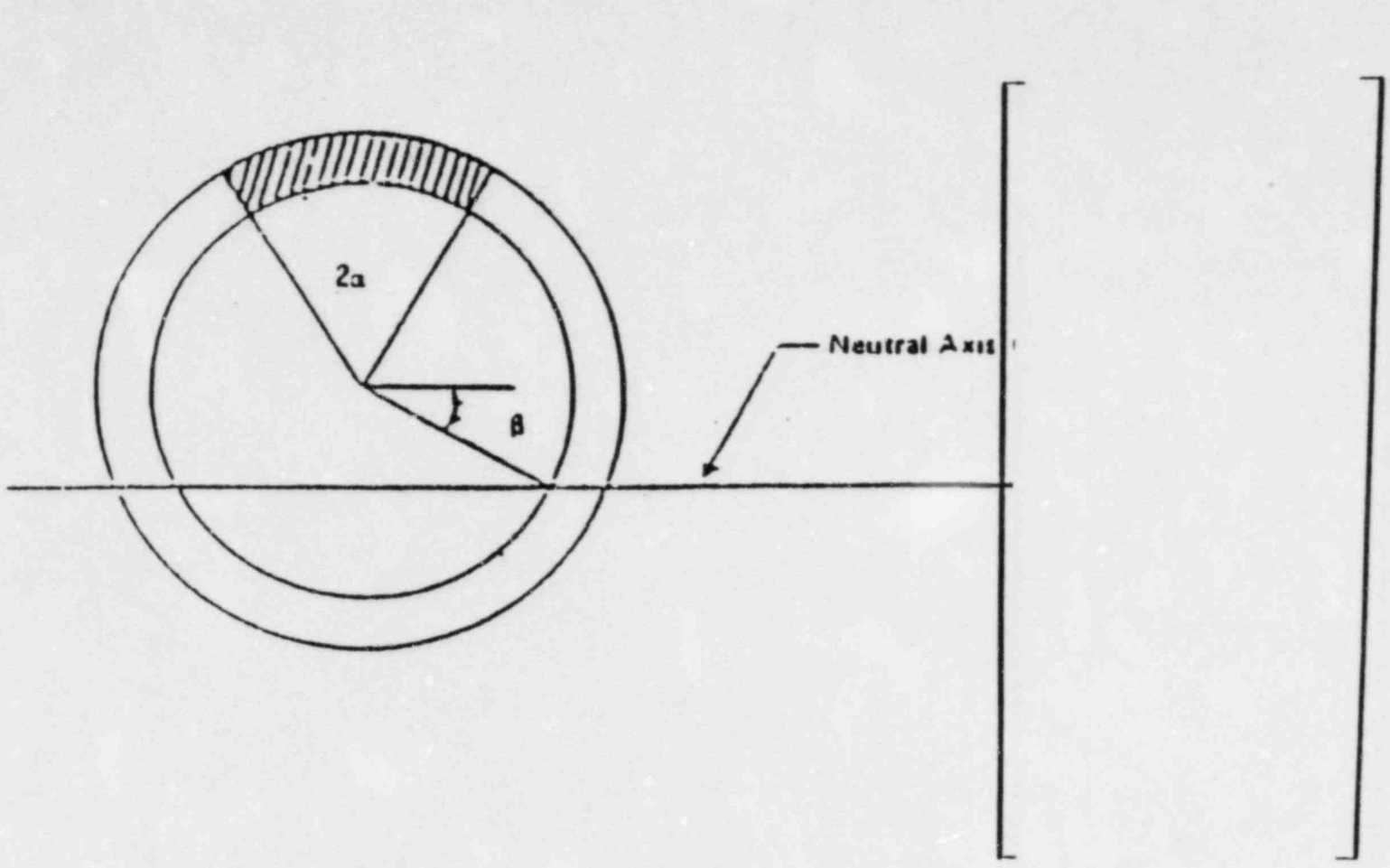

FIGURE A-1 EQUILIBRIUM OF HORIZONTAL FORCES

APPENDIX B

VERIFICATION OF THE[ ]RESULTS a,c,e

The purpose of the verification presented herein is to assure the correctness of the fracture mechanics analysis for the pipe. Both the K_I values due to the pure axial stretching and the pure bending are investigated. The outer fiber stresses corresponding to the maximum applied bending moment are investigated also.

(1) <u>The K_I for a circumferentially cracked pipe subjected to a uniform tensile load</u>

The elastic solution for this problem has been studied by Folias [B-1] and others. Under the present geometrical and loading conditions, the K_I is given by

+a,c,e

[ ]

+a,c,e

(B-4)

[+a,c,e

]

Substituting [ ] +a,c,e
ksi√in. The difference between the results by Eq. (B-3) and the VCE method is 2.3 percent.

(2) K_I due to pure bending

The K_I for a circumferentially cracked pipe subjected to bending may be estimated by taking the average of that produced by the tensile outer fiber stress, σ_b, and by the fiber stress at the location of the crack tip, σ'. These stresses are shown in Figure B-1. The relation between σ_b and σ' is given by

$$\sigma' = \sigma_b \cos \alpha \qquad \text{(B-5)}$$

where α=crack angle (see Figure B-1). Therefore the K_I due to bending is

$$K_{I,b} = [\quad] \qquad \text{(B-6)}$$ +a,c,e

Inserting Eq. B-5 into Eq. B-6 and taking [+a,c,e
], one obtains:

$$K_{I,b} = [\quad] \qquad \text{(B-7)}$$ +a,c,e

A pure bending load with [

]

was used for the[ ]analysis and the [ ] produced +a,c,e
[ ] This [ ] is converted to the +a,c,e
[ ] of [ ]. +a,c,e

Substituting [+a,c,e
] The difference in this case is about 6 percent.

It need be noted that Eqs. B-3 and B-7 are valid only for the elastic deformation. When loads increase the linear elastic theory underestimates the [ ] The deviation is considerable when +a,c,e
large plastic zone in the crack tip region is developed. However, these equations can be used for reference purpose. This means that the actual [ ] should be always greater than those given by Eqs. B-1 and +a,c,e
B-6. This condition or requirement is met for the present analysis.

(3) Check on the Outer fiber stress

In addition to examining the [ ]values, the axial stress +a,c,e
which directly relates to the open mode of fracture is examined herein. Only the outer fiber stress on the tension side is checked. Since there is no plastic deformation in the region remote from the crack up to [ ]in-kip, the bending stress below this load level can be computed by

$$\sigma_b = \frac{M}{I} z \qquad (B\text{-}8)$$

where M = bending moment
I = moment of initia
z = distance from the neutral axis.

Based on the geometrical data employed in the present analysis, [+a,c,e
.] For [ ] in-kip (which is the bending moment +a,c,e
corresponding to load [+a,c,e

] In addition to

the bending stress, there is an axial stress, σ_a, of [ ] ksi +a,c,e
constantly acting on the pipe. Therefore, the combined fiber stress at the Guassian point investigated is

$$\sigma_{tot} = \sigma_a + \sigma_b$$

$$= [\quad] \qquad +a,c,e$$

The corresponding stress given by [ ] is [ ] ksi. The error is +a,c,e
1.7 percent.

Reference

B-1 Folias, E. S., "On the Effect of Initial Curvature on Cracked Flat Sheets," Int. J. of Frac. Mech., Vol. 5, 1969, pp. 327-346.

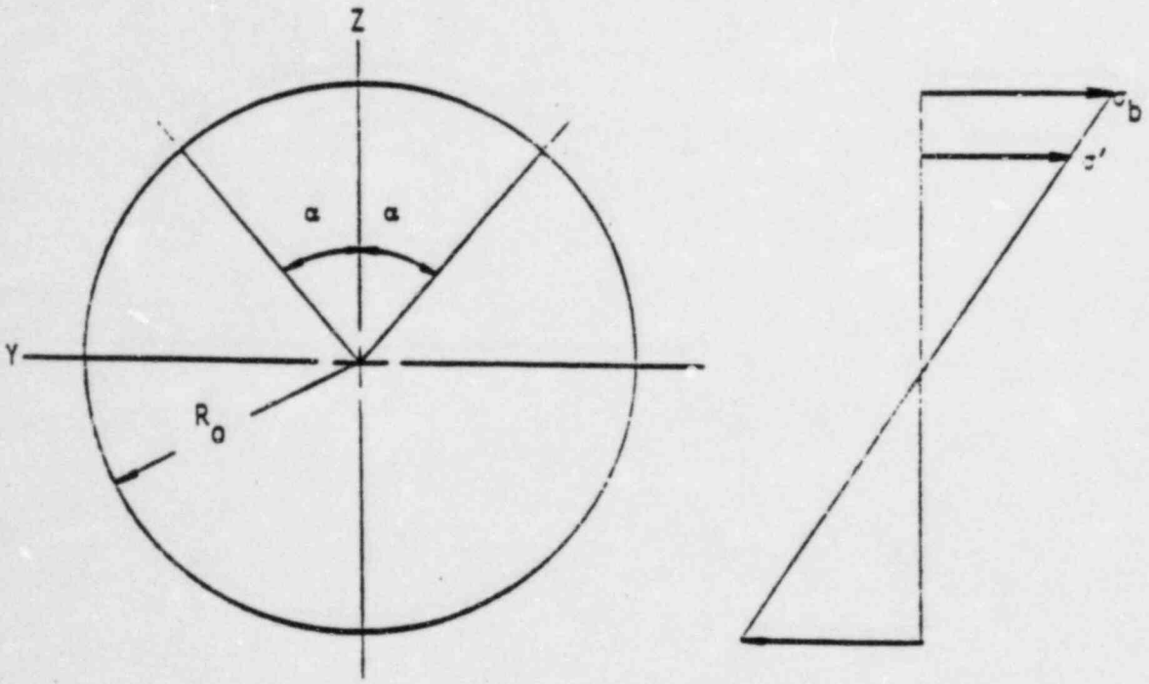

$$\sigma_b = \frac{M}{I} R_o$$

$$\sigma' = \frac{M}{I} (R_o \cos\alpha) = \sigma_b \cos\alpha$$

α = crack angle

Figure B-1 Auxiliary diagram for derivation of Equation B-6.